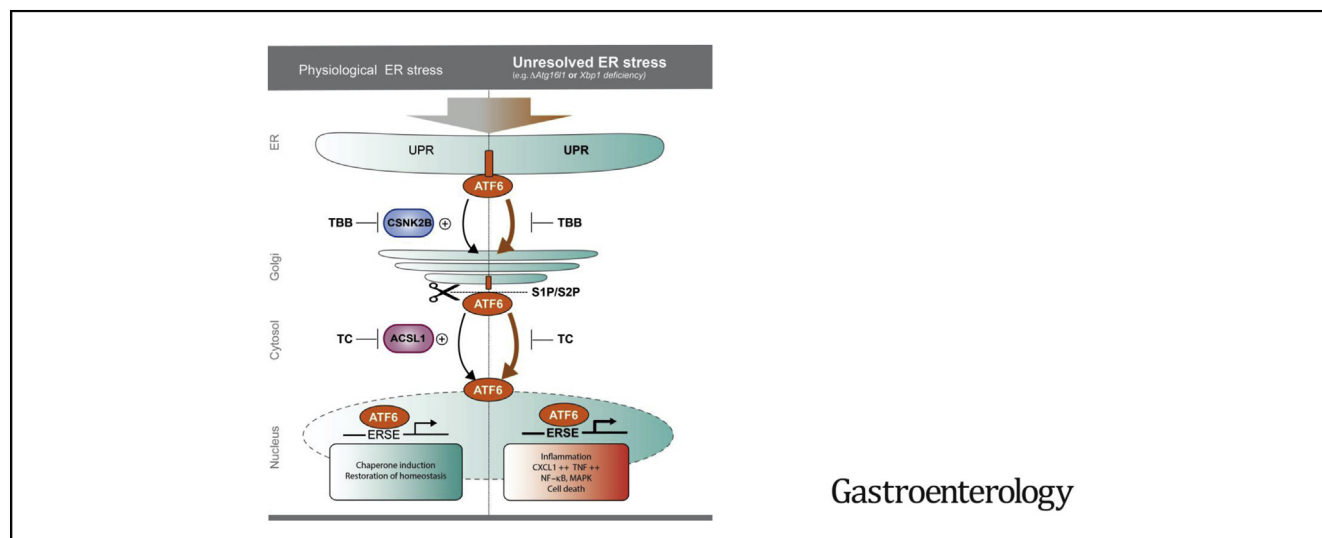


Activating Transcription Factor 6 Mediates Inflammatory Signals in Intestinal Epithelial Cells Upon Endoplasmic Reticulum Stress



Stephanie T. Stengel,¹ Antonella Fazio,¹ Simone Lipinski,¹ Martin T. Jahn,² Konrad Aden,^{1,3} Go Ito,^{1,4} Felix Wottawa,¹ Jan W. P. Kuiper,¹ Olivia I. Coleman,⁵ Florian Tran,^{1,3} Dora Bordoni,¹ Joana P. Bernardes,¹ Marlene Jentzsch,¹ Anne Luzius,¹ Sandra Bierwirth,⁵ Berith Messner,¹ Anna Henning,¹ Lina Welz,¹ Nassim Kakavand,¹ Maren Falk-Paulsen,¹ Simon Imm,¹ Finn Hinrichsen,¹ Matthias Zilbauer,⁶ Stefan Schreiber,³ Arthur Kaser,⁷ Richard Blumberg,⁸ Dirk Haller,⁵ and Philip Rosenstiel¹

¹Institute of Clinical Molecular Biology, Christian-Albrechts-University and University Hospital Schleswig-Holstein, Campus Kiel, Kiel, Germany; ²RD3 Marine Microbiology, GEOMAR Helmholtz Centre for Ocean Research Kiel, Germany; ³Department of Internal Medicine I., Christian-Albrechts-University and University Hospital Schleswig-Holstein, Campus Kiel, Kiel, Germany; ⁴Department of Gastroenterology and Hepatology, Tokyo Medical and Dental University, Tokyo, Japan; ⁵Nutrition and Immunology, Technische Universität München, Freising, Germany; ⁶Department of Pediatrics, University of Cambridge, Addenbrooke's Hospital, Cambridge, UK; ⁷Division of Gastroenterology and Hepatology, Department of Medicine, Addenbrooke's Hospital, University of Cambridge, Cambridge, UK; and ⁸Gastroenterology Division, Department of Medicine, Brigham and Women's Hospital, Harvard Medical School, Boston, MA



BACKGROUND & AIMS: Excess and unresolved endoplasmic reticulum (ER) stress in intestinal epithelial cells (IECs) promotes intestinal inflammation. Activating transcription factor 6 (ATF6) is one of the signaling mediators of ER stress. We studied the pathways that regulate ATF6 and its role for inflammation in IECs. **METHODS:** We performed an RNA interference screen, using 23,349 unique small interfering RNAs targeting 7783 genes and a luciferase reporter controlled by an ATF6-dependent ERSE (ER stress-response element) promoter, to identify proteins that activate or inhibit the ATF6 signaling pathway in HEK293 cells. To validate the screening results, intestinal epithelial cell lines (Caco-2 cells) were transfected with small interfering RNAs or with a plasmid overexpressing a constitutively active form of ATF6. Caco-2 cells with a CRISPR-mediated disruption of autophagy related 16 like 1 gene (*ATG16L1*) were used to study the effect of ATF6

on ER stress in autophagy-deficient cells. We also studied intestinal organoids derived from mice that overexpress constitutively active ATF6, from mice with deletion of the autophagy related 16 like 1 or X-Box binding protein 1 gene in IECs (*Atg16l1*^{ΔIEC} or *Xbp1*^{ΔIEC}, which both develop spontaneous ileitis), from patients with Crohn's disease (CD) and healthy individuals (controls). Cells and organoids were incubated with tunicamycin to induce ER stress and/or chemical inhibitors of newly identified activator proteins of ATF6 signaling, and analyzed by real-time polymerase chain reaction and immunoblots. *Atg16l1*^{ΔIEC} and control (*Atg16l1*^{fl/fl}) mice were given intraperitoneal injections of tunicamycin and were treated with chemical inhibitors of ATF6 activating proteins. **RESULTS:** We identified and validated 15 suppressors and 7 activators of the ATF6 signaling pathway; activators included the regulatory subunit of casein kinase 2 (CSNK2B) and acyl-CoA synthetase

long chain family member 1 (ACSL1). Knockdown or chemical inhibition of CSNK2B and ACSL1 in Caco-2 cells reduced activity of the ATF6-dependent ERSE reporter gene, diminished transcription of the ATF6 target genes *HSP90B1* and *HSPA5* and reduced NF- κ B reporter gene activation on tunicamycin stimulation. *Atg16l1*^{ΔIEC} and or *Xbp1*^{ΔIEC} organoids showed increased expression of ATF6 and its target genes. Inhibitors of ACSL1 or CSNK2B prevented activation of ATF6 and reduced CXCL1 and tumor necrosis factor (TNF) expression in these organoids on induction of ER stress with tunicamycin. Injection of mice with inhibitors of ACSL1 or CSNK2B significantly reduced tunicamycin-mediated intestinal inflammation and IEC death and expression of CXCL1 and TNF in *Atg16l1*^{ΔIEC} mice. Purified ileal IECs from patients with CD had higher levels of ATF6, CSNK2B, and HSPA5 messenger RNAs than controls; early-passage organoids from patients with active CD show increased levels of activated ATF6 protein, incubation of these organoids with inhibitors of ACSL1 or CSNK2B reduced transcription of ATF6 target genes, including *TNF*. **CONCLUSIONS:** Ileal IECs from patients with CD have higher levels of activated ATF6, which is regulated by CSNK2B and HSPA5. ATF6 increases expression of TNF and other inflammatory cytokines in response to ER stress in these cells and in organoids from *Atg16l1*^{ΔIEC} and *Xbp1*^{ΔIEC} mice. Strategies to inhibit the ATF6 signaling pathway might be developed for treatment of inflammatory bowel diseases.

Keywords: IBD; Inflammation; Signal Transduction; Gene Expression.

The endoplasmic reticulum (ER) is a tightly controlled cellular compartment for synthesis and folding of secretory proteins. Accumulation of unfolded/misfolded proteins within the ER provokes an unfolded protein response (UPR) with the aim to reduce ER stress and restore homeostasis. Unresolved ER stress can lead to excessive UPR activation, which can be inflammatory and ultimately lead to programmed cell death.¹ Three main arms govern the ER-stress-induced response in mammalian cells, regulated by 3 key molecules, respectively: IRE1 α (endoribonuclease inositol-requiring enzyme 1 α), PERK (protein kinase RNA-like ER kinase), and ATF6 α .^{2,3} These 3 proximal transmembrane sensors are activated by dissociation of the ER chaperone glucose-regulated protein 78 (GRP78) in favor of binding to misfolded proteins. Unbound ATF6 α translocates to the Golgi network, where it undergoes regulated intramembrane proteolysis mediated by the site 1 and site 2 protease (S1P/S2P). The released cytosolic N-terminal portion of ATF6 α migrates to the nucleus and induces the expression of genes containing ER-stress response elements (ERSE-I and -II) (eg, GRP78).⁴ Recent findings indicate that activation of the UPR induces macroautophagy and that autophagy in turn is able to alleviate the UPR.⁵⁻⁹ A strong link for an impaired UPR/autophagy crosstalk has been identified in the etiopathogenesis of inflammatory bowel disease (IBD), by both functional and genetic evidence.^{7,8,10-12} Conditional deletion of XBP1 in the intestinal epithelium leads to paradoxical activation of ER stress and a

WHAT YOU NEED TO KNOW

BACKGROUND AND CONTEXT

Endoplasmic reticulum stress in intestinal epithelial cells promotes intestinal inflammation. Activating transcription factor 6 (ATF6) is one of the cellular mediators of the ER stress response.

NEW FINDINGS

Ileal epithelial cells from patients with CD have higher levels of activated ATF6, which is regulated by CSNK2B and ACSL1. ATF6 increases expression of tumor necrosis factor and other inflammatory cytokines in response to endoplasmic reticulum stress in intestinal cells.

LIMITATIONS

This study was performed in cell lines, tissues from patients, and mice; further studies of this pathway are needed in humans.

IMPACT

Strategies to inhibit ATF6 signaling pathway might be developed for treatment of inflammatory bowel diseases.

spontaneous enteritis in mice.⁸ Likewise, mice with a conditional intestinal epithelial deletion of the Crohn's disease (CD) risk gene autophagy related 16 like 1 (ATG16L1), a core component of the autophagic machinery, display signs of unresolved ER stress, impaired Paneth cell architecture and suffer from spontaneous, age-dependent onset of ileitis.¹³ The models share increased proinflammatory signals via nuclear factor (NF)- κ B, high levels of tumor necrosis factor (TNF) α secretion, increased necroptotic epithelial cell death, and accumulation of IRE1 α ,^{5,13,14} reflecting molecular alterations observed in patients with IBD.

Surprisingly little is known about the executioners of the inflammatory signaling under conditions of hyperactivated ER stress. Importantly, although the downstream transcriptional program induced by ATF6 α signaling has been extensively studied in the context of ER homeostasis,^{15,16} our knowledge regarding the exact regulatory network of the ATF6 branch within the intestinal epithelium is still limited. We hypothesized that modulation of ATF6 α function might counteract detrimental signals of aggravated ER stress in IECs, specifically in conditions of genetically disturbed autophagy.

Abbreviations used in this paper: ACSL1, Acyl-CoA Synthetase Long Chain Family Member 1; ATF6, activating transcription factor 6; Atg16l1, autophagy related 16 like 1; CD, Crohn's disease; CSNK2B, casein kinase 2 beta; ER, endoplasmic reticulum; ERSE, ER-stress response elements; GRP78, glucose-regulated protein 78 kDa; IBD, inflammatory bowel disease; IECs, intestinal epithelial cells; IRE1, endoribonuclease inositol-requiring enzyme 1; mRNA, messenger RNA; NF- κ B, nuclear factor kappaB; PCR, polymerase chain reaction; S1P/S2P, site 1/2 protease; SI, small intestine; siRNA, small interfering RNA; TBB, 4,5,6,7-Tetrabromo-2-azabenzimidazole; TC, Triacsin C; TNF, tumor necrosis factor; UPR, unfolded protein response; WT, wild type; Xbp1, X-box binding protein 1.

Most current article

© 2020 by the AGA Institute. Published by Elsevier Inc. This is an open access article under the CC BY-NC-ND license (<http://creativecommons.org/licenses/by-nc-nd/4.0/>).

0016-5085

<https://doi.org/10.1053/j.gastro.2020.06.088>

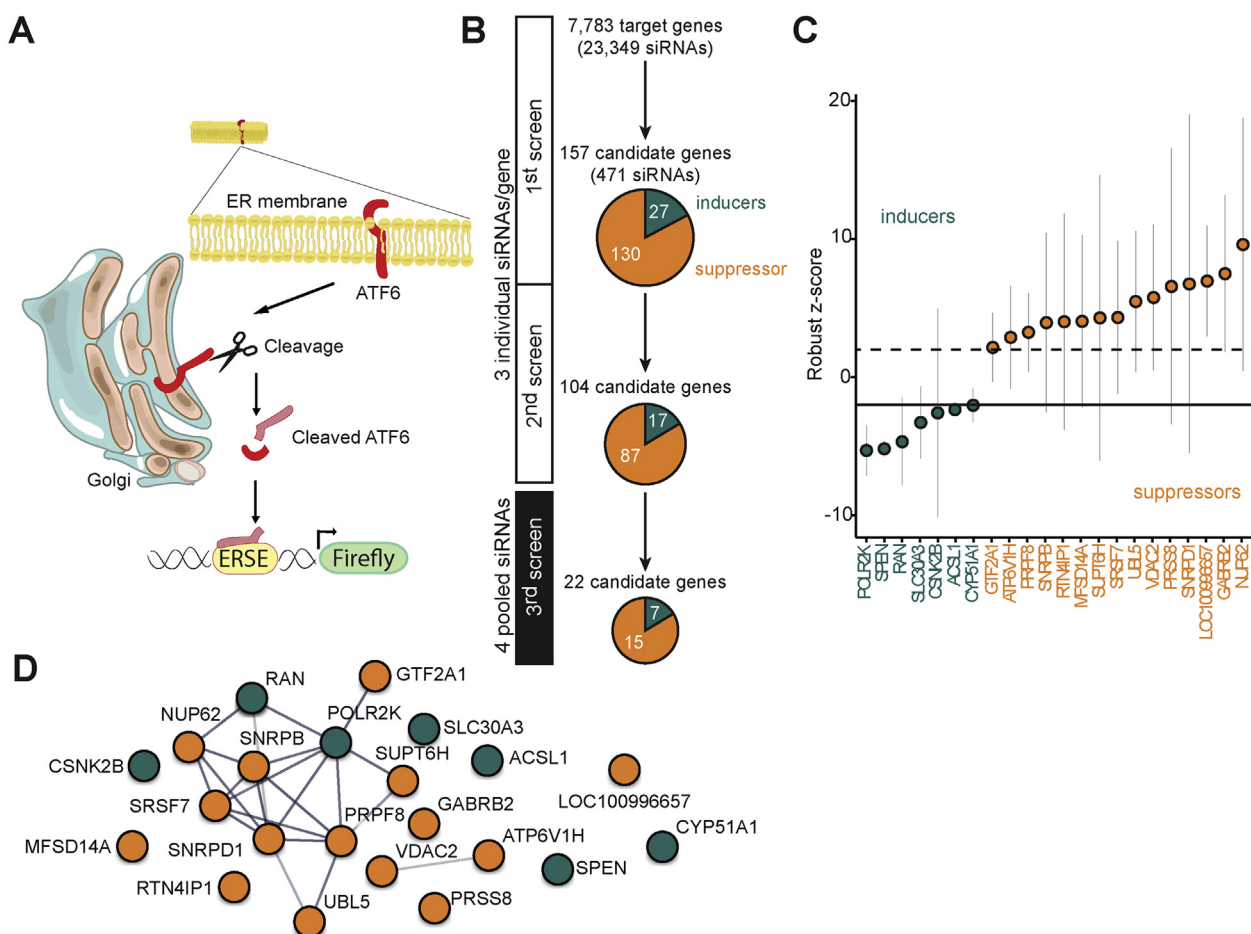


Figure 1. Systematic siRNA screening reveals modulators of ATF6 α activation. (A) Schematic representation of the screening approach. (B) Screening procedure and number of candidates at different screening stages. In the primary and secondary screens each gene was targeted with 3 individual siRNAs tested separately. Pools of 4 siRNAs were used for the third screen. Candidate genes with an inducing or repressing effect on ATF6 activation are indicated in *green* or *orange*, respectively. (C) Final set of 22 candidates after the third screen. Bars depict mean and 95th confidence interval (3 replicates). (D) STRING Network of candidate genes (third screen). Only interactions with a confidence score >0.4 were considered. Inducers depicted in *green*, repressors shown in *orange*. (E–H) ERSE promoter activity quantified by dual luciferase reporter assay in HEK-293 cells. N = 6. Cells were exposed to tunicamycin (5 μ g/mL) and small molecule agents for 24 hours. Depicted data representative of 3 independent experiments. Statistical analysis was performed using 1-way analysis of variance together with Tukey post hoc test. TPEN, N,N,N',N'-Tetrakis(2-pyridylmethyl)ethylenediamine; CM, Camostat mesylate; Sim, Simvastatin.

In this study, we set out to systematically understand modulators of ATF6 α signaling using a stringent high-throughput RNA interference screening. Among the validated hits, 2 upstream co-activators of ATF6 α signaling were identified and further validated: Acyl-CoA Synthetase Long Chain Family Member 1 (ACSL1) and the casein kinase 2 beta (CSNK2B). Using primary murine intestinal organoid cultures, we show that impairment of autophagy or unresolved ER stress in IECs results in the compensatory up-regulation of the ATF6 α branch, which we link to enhanced proinflammatory signaling and cytokine secretion, which could be restricted by inhibition of ACSL1 or CSNK2B *in vitro* and *in vivo*. Our findings point to upstream inhibition of ATF6 α as a novel therapeutic strategy to overcome detrimental proinflammatory effects of failing autophagy and the UPR in IECs.

Materials and Methods

Cell Culture and Reagents

Information on cell culture and reagents can be found in the [supplementary material](#).

Cultivation of Murine Small Intestine Organoids

Crypts were isolated from mouse small intestine (SI) by EDTA-based $\text{Ca}^{2+}/\text{Mg}^{2+}$ chelation and intestinal organoids were cultivated as described by Sato et al.¹⁷

Culture of Human Intestinal Organoids

Human intestinal biopsy specimens were obtained from patients who underwent endoscopic examination. The study was approved by the Ethics Committee of the Medical Faculty, University Kiel (vote B231/98) and written informed consent was obtained from each patient prior to study related

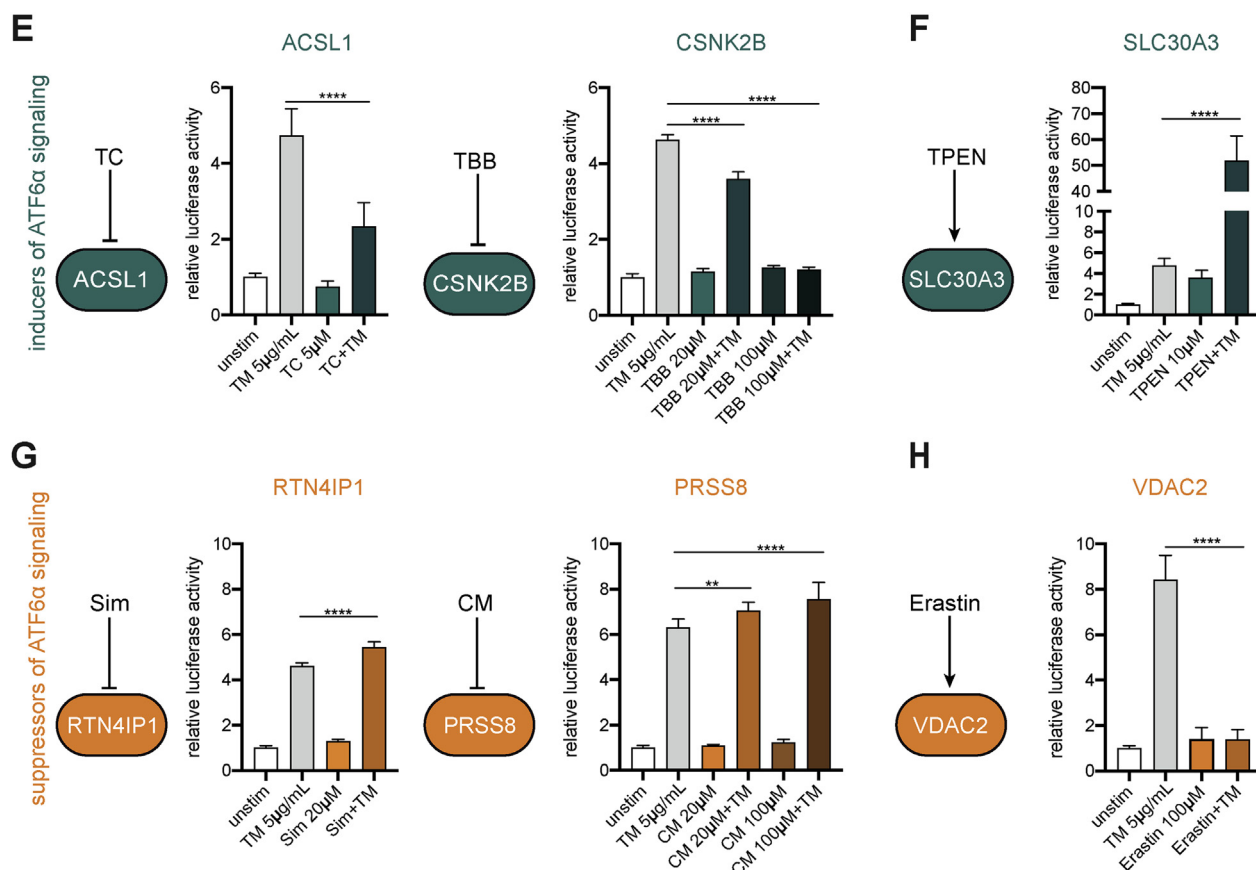


Figure 1. Continued.

procedures. Isolation of the crypts and establishment of intestinal organoids were performed as described.¹⁸ Organoids were passaged every 6 to 7 days. For all experiments, organoids were used at passage 3 to 5.

High-Throughput RNA Interference Screening Procedure

A total of 23,349 unique small interfering RNAs (siRNAs) targeting 7783 genes were screened using the Silencer Human Druggable Genome siRNA library V3 (Ambion, Austin, TX). HEK-293 cells were reverse transfected with either single siRNAs (Ambion; primary and secondary screen) or siRNA pools (siGENOME; SMARTpool; Dharmacon, Lafayette, LA; tertiary screen) complexed with siPORT Amine (Ambion) as described.¹⁹

Dual Luciferase Reporter Assays

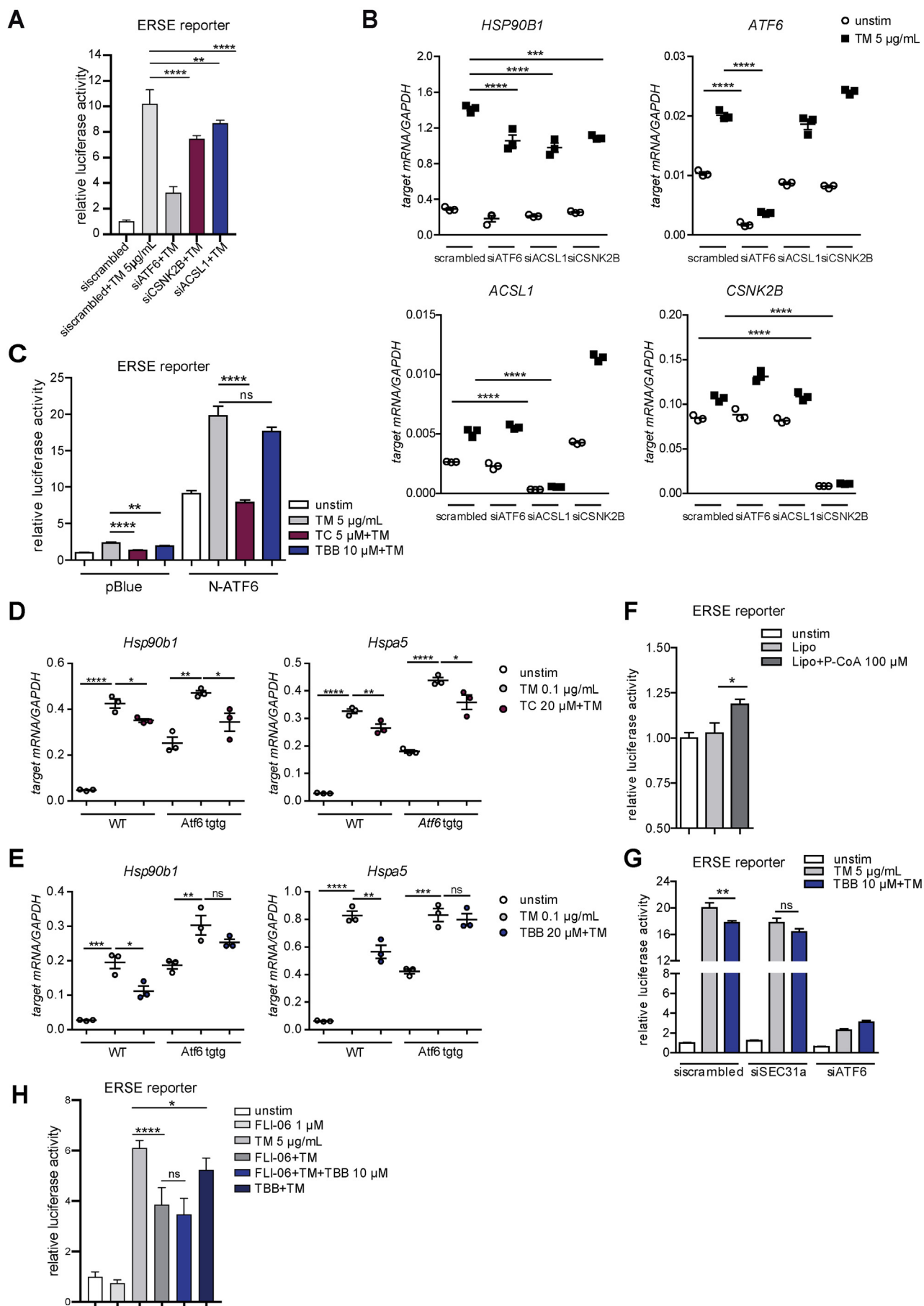
Plasmid-encoded ERSE-dependent firefly luciferase (pGL3-ERSE, 12 ng/well) and a constitutive thymidine-kinase driven *Renilla* luciferase were used in a dual luciferase assay (Clontech, 3 ng/well) to assay ATF6/ERSE activation. For quantification of the NF- κ B promoter activity, a reporter system based on NF- κ B responsive promoter elements driving expression of the Firefly luciferase (40 ng/well) was used.¹⁹ For all luciferase reporter assays, the fold change is depicted. For calculating the fold change, unstimulated wild-type (WT) controls were set to 1.

RNA Extracts and Quantitative Real-Time Polymerase Chain Reaction

Total RNA was isolated using the RNeasy kit (Qiagen, Hilden, Germany). Total RNA was reverse-transcribed to complementary DNA using the Maxima H Minus First Strand cDNA Synthesis kit (Thermo Scientific, Waltham, MA). Quantitative real-time polymerase chain reaction (PCR) was performed using the TaqMan Gene Expression Master Mix (Applied Biosystems, Foster City, CA) and analyzed by the 7900HT Fast Real-Time PCR System (Applied Biosystems). The following TaqMan assays (Applied Biosystems) were used: *ACSL1*(00960561), *CSNK2B*(00365635), *ATF6*(00232586), *HSP90B1*(00427665), *DNAJC3*(00534483), *Hsp90b1*(00441926), *Hspa5*(00517690), and *Tnf*(00443258). Relative transcript levels were determined using the indicated housekeeper and the standard curve method.²⁰

Immunoblotting

Western blots were performed as described.¹⁴ α -ATF6 antibody was purchased from Acris (Rockville, MD) (SM7007P), α -GRP78 from Abcam (Cambridge, UK) (ab21685), α -ATG16L1 from CST (Danvers, MA) (#8089), GRP94 from CST (#2104), α -p100/p52 from CST (#52583), α -p-p65 from Abcam (ab86299), α -p65 from CST (#82429), α -p38, and α -p-p38 from CST (#9212 and #9211, respectively).



Histopathological Analyses of Murine SI Tissue

Histological scoring was performed in a blinded fashion. The histological score displays the combined score of inflammatory cell infiltration, cell death (TUNEL) and tissue damage as described elsewhere.⁵

Mice

Villin(V)-cre⁺; Xbp1^{fl/fl} (Xbp1^{ΔIEC}), Villin(V)-cre⁺; Atg16l1^{fl/fl} (Atg16l1^{ΔIEC})⁵ mice, backcrossed for at least 6 generations on a C57BL/6 background, were used at an age of 8 to 20 weeks. All mice were maintained in a specific pathogen-free facility. All experiments were performed in accordance with the guidelines for Animal Care of Kiel University and in conformity to national and international laws and policies and with appropriate permissions (acceptance no. V242-7224.121-33).

In Vivo Treatment of Mice

Atg16l1^{ΔIEC} or Atg16l1^{fl/fl} mice were treated with 1mg/kg bodyweight tunicamycin or dimethyl sulfoxide intraperitoneally (IP) for 24 hours or 72 hours before being killed. Groups of mice received 2.5 μg/g bodyweight Triacsin C (TC) or 40 μg/g bodyweight CX-4945 IP, respectively, at 0, 24, and 48 hours post tunicamycin injection (72-hour experiment) or once at 0 hour (24-hour experiment). This animal experiment was approved by the Animal Investigation Committee of the University Hospital Schleswig-Holstein (acceptance no. V242-32647/2018 [59-7/18]).

Statistics

Statistical analysis was performed using the GraphPad Prism 5 software package (GraphPad Software Inc., La Jolla, CA). Unless otherwise stated, the Student unpaired *t* test was performed. Data are shown as mean ± standard error of the mean (SEM). In case multiple groups were compared, the analysis of variance with post hoc Tukey's test was used for statistical analysis. A *P* value of ≤ .05 was considered as significant (*). A *P* value of ≤ .01 was considered as strongly significant (**) and *P* value of ≤ .001 as highly significant (***). **** indicates *P* value ≤ .0001.

Results

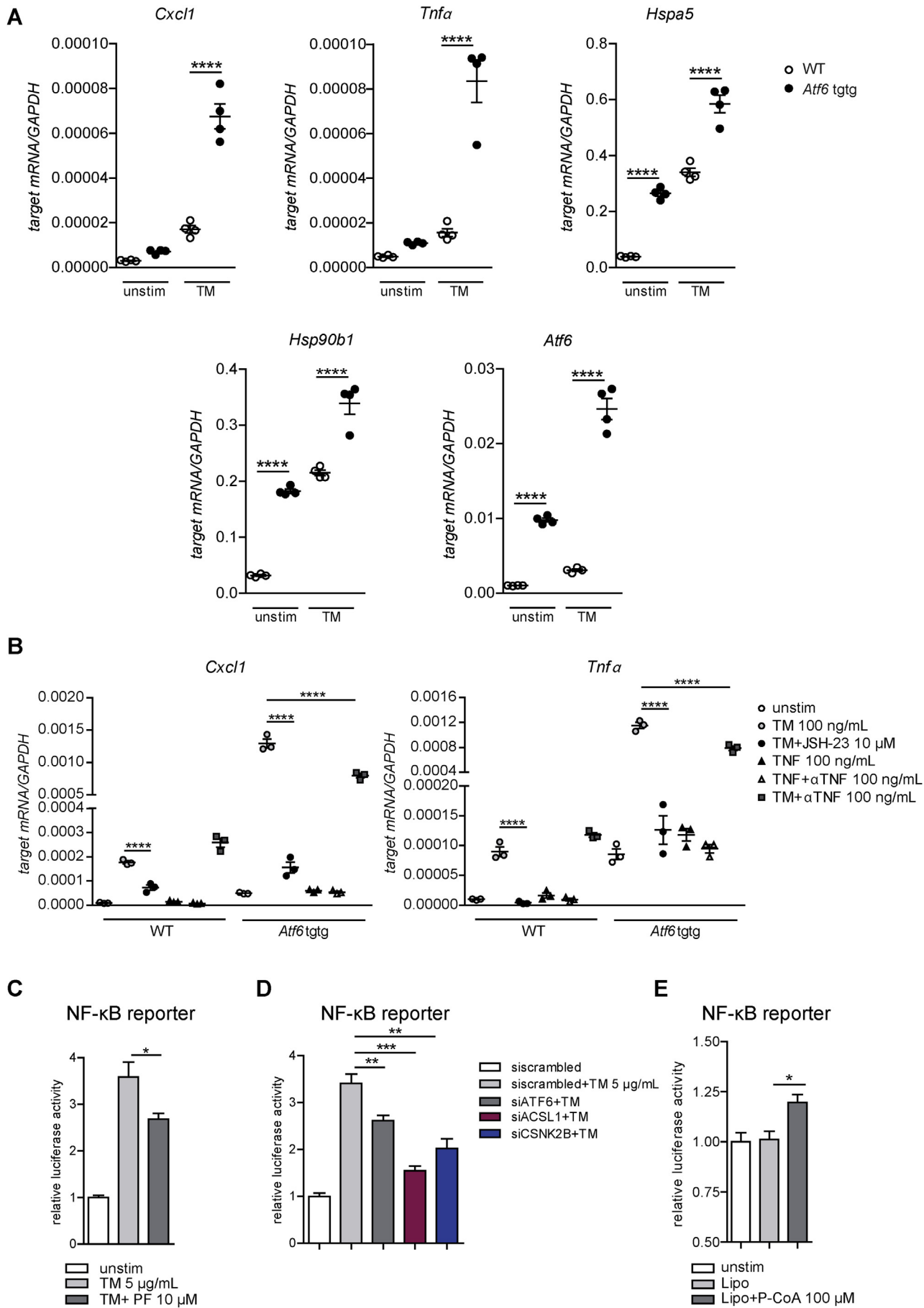
Identification and Network Analysis of ATF6α Signaling Modulators

To identify modulators of the ATF6α signaling pathway, we targeted 7783 genes using a commercially available “druggable” genome siRNA library. The screen was performed in human embryonic kidney cells (HEK-293) transfected with siRNA and a luciferase reporter construct driven by an ATF6-specific ERSE cassette (Figure 1A).⁴ Luciferase activity was measured 24 hours after stimulation with the ER-stress inducer tunicamycin (5 μg/mL), which inhibits N-glycosylation. Each transcript was targeted using 3 different siRNAs, resulting in a total number of 23,349 assays for ATF6 activation (Figure 1B). Genes with a normalized, averaged fold-induction higher than 2.0 or lower than −2.0 were considered as candidate genes. To validate the findings, the 157 genes (Supplementary Table 1A) were rescreened using the same experimental setup. The remaining 104 candidate genes (Supplementary Table 1B) were subjected to a third screen using pools of 4 independent siRNAs per transcript (Figure 1B). This stringent approach resulted in 22 hits (Supplementary Table 1C), comprising 15 suppressors and 7 activators of ATF6α signaling (Figure 1B and C). A protein interaction network (STRING) analysis revealed an increased connectivity from the primary to the tertiary screen (primary screen: average local clustering coefficient 0.367, *P* value 0.00147; third screen: 0.469 and 1.15×10^{-8} , respectively).

Validated siRNA-mediated Cellular ER-stress Regulation by Selected Individual Candidates Is Phenocopied by Chemical Interference

From the regulatory network of 22 validated ATF6α signaling modulators, we selected 6 candidates for further functional characterization based on their (1) known biological function, (2) cellular localization (ER, Golgi, nucleus), (3) availability of specific inhibitors/inducers, (4) antibody availability, and (5) available mouse models (Supplementary Figure 1B, Supplementary Table 1D). To independently validate the siRNA-mediated effects, we used

Figure 2. CSNK2B controls ATF6α signaling upstream of intramembrane cleavage. (A and B) siRNA-mediated knockdown of ACSL1 (siACSL1), CSNK2B (siCSNK2B), and ATF6α (siATF6) in Caco-2 cells. Scrambled = nontargeting control siRNA. (A) ERSE promoter activity quantified by dual luciferase reporter assays. After 24 hours, cells were stimulated with 5 μg/mL tunicamycin (TM) for additional 24 hours. (B) mRNA levels of ATF6α target HSP90B1 were measured by quantitative PCR (n = 3) 24 hours after TM stimulation. (C) Effects of TC and TBB treatment on ERSE promoter activity in Caco-2 cells quantified by dual luciferase reporter assays. Cells transfected either with N-ATF6α or with the empty plasmid (blue) and stimulated with tunicamycin and inhibitors (24 hours). (D and E) Transcript levels of Hsp90b1 and Hspa5 in WT and Atf6α transgenic (Atf6 tg/tg) SI organoids treated with tunicamycin (0.1 μg/mL) and TC (D) or TBB (E) for 24 hours. (F) Caco-2 cells were stimulated with lipofectamine-complexed Palmitoyl coenzyme A (100 μM) or lipofectamine alone (Lipo) for 24 hours and ERSE dual luciferase reporter activity was measured. (G) ERSE promoter activity in Caco-2 cells on siRNA-mediated depletion of SEC31a (siSEC31a). (H) ER-Golgi transport was inhibited in Caco-2 cells with FLI-06 (1 μM) in presence or absence of tunicamycin and TBB, respectively. Cells stimulated for 24 hours. ERSE promoter activity quantified by dual luciferase reporter assay. Shown data representative of 3 independent experiments. For statistical analysis, 1-way analysis of variance together with Tukey post hoc test was performed.



corresponding chemical inhibitors or inducers (Figure 1E–H). Direct inhibition of the identified ATF6 α signaling inducers ACSL1 (Acyl-CoA Synthetase Long Chain Family Member 1) and CSNK2B (Casein Kinase 2 β) using TC and 4,5,6,7-Tetrabromo-2-azabenzimidazole (TBB), respectively, significantly reduced ERSE promoter activity upon ER-stress induction (Figure 1E). Treatment of cells with N,N,N',N'-Tetrakis (2-pyridylmethyl)ethylenediamine (TPEN), a Zn²⁺ chelator, known to increase the expression of the identified ATF6 α inducer *SLC30A3*,²¹ elevated the activity of the ATF6 α (Figure 1F). Inhibition of the serine protease 8 (PRSS8) activity by Camostat mesylate (CM) augmented ATF6 α signaling (Figure 1G). Indirect inhibition of RTN4IP1 (Reticulon 4 Interacting Protein 1) signaling with Simvastatin (Sim), which blocks RhoA signaling, a downstream target of RTN4 (Reticulon 4)²² verified RTN4IP1 as a repressor of ATF6 α signaling (Figure 1G). Treatment of cells with the VDAC2 (voltage dependent anion channel 2) binding small molecule Erastin, known to induce VDAC2 expression,²³ diminished ATF6 α signaling and confirmed VDAC2 as repressor of this signaling branch (Figure 1H).

ACSL1 and CSNK2B Act on Distinct Steps of ATF6 α Signaling in IECs

To further confirm the relevance of *ACSL1* and *CSNK2B* in the intestinal epithelium, we silenced *ACSL1* and *CSNK2B* in the Caco-2 cells using siRNA transfection (for knockdown efficiency, see Supplementary Figure 2A). This resulted in significantly reduced ERSE promoter activity (Figure 2A) and reduced messenger RNA (mRNA) levels of the canonical ATF6 α -target gene *HSP90B1* (*GRP94*) after tunicamycin stimulation (Figure 2B).

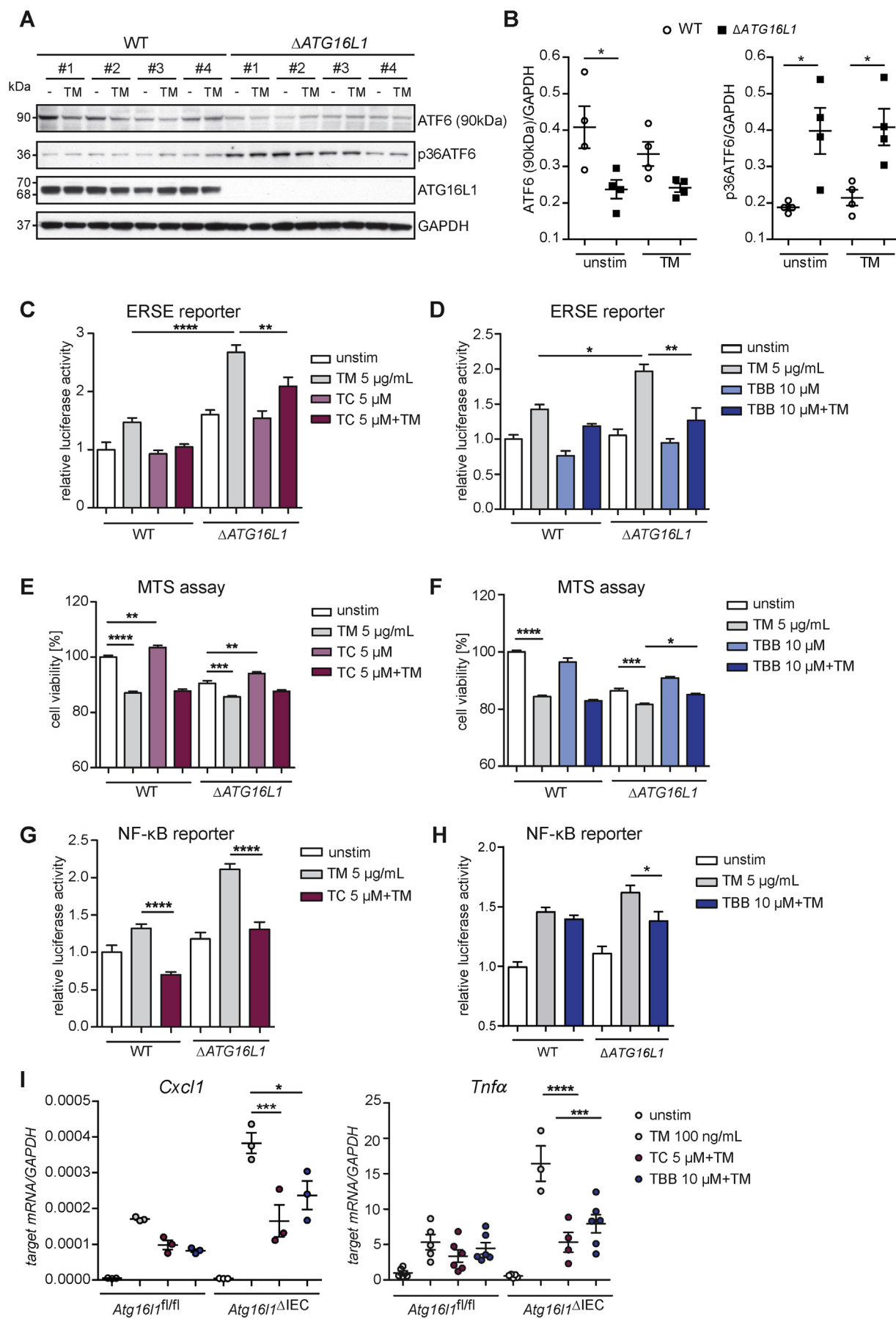
To address the molecular mechanism how ACSL1 and CSNK2B act on ATF6 α signaling, we first transfected Caco-2 cells either with a plasmid encoding the transcriptionally active N-terminal ATF6 α fragment.²⁴ In this model, influence of an inhibitor would point to an effect downstream of the S1/2P-dependent intramembrane proteolysis of ATF6 α . We found that ACSL1 inhibition by TC repressed ERSE activation in cells overexpressing N-terminal ATF6 α , whereas treatment with the CSNK2B inhibitor TBB did not inhibit ERSE-dependent reporter gene activity (Figure 2C). Similarly, in intestinal organoids derived from transgenic mice overexpressing the activated form of ATF6 α (Villin-Cre::nAtf6 α tg carrying a loxP-STOP-loxP cassette in front of the transgene, termed Atf6tgtg

hereafter),²⁴ TBB treatment did not diminish mRNA levels of *Atf6 α* target genes (*Hsp90b1*, *Hspa5*) upon ER-stress induction by tunicamycin and at baseline. In contrast, inhibition of ACSL1 with TC resulted in reduced mRNA levels of *Hsp90b1* (*Grp94*) and *Hspa5* (*Grp78*) (Figure 2D and E). These results imply that ACSL1 mediates its co-activating effect on ATF6 α signaling downstream of the cleavage event at the Golgi apparatus. Treatment of IECs with Palmitoyl coenzyme A, product of the enzymatic reaction catalyzed by ACSL1, caused increased ERSE reporter activity (Figure 2F) supporting the role of ACSL1 as inducer of ATF6 α signaling. Importantly, the lack of effect of the CSNK2B inhibitor TBB on Atf6tgtg-induced signaling implies that CSNK2B regulates ATF6 α signaling upstream of the intramembrane proteolysis. Koreishi et al²⁵ demonstrated previously that the casein kinase 2 (CK2), composed of CSNK2B and CSNK2A, phosphorylates the COPII constituent Sec31, thereby facilitating ER-Golgi trafficking. As it was shown that ATF6 α trafficking is dependent on COPII vesicles,²⁶ we hypothesized that CSNK2B might be involved in the transport of ATF6 α from the ER to the Golgi apparatus. Indeed, depletion of SEC31 by siRNA in IECs abolished the inhibitory effect of TBB on ERSE reporter gene activity (Figure 2G). In further support of these findings, inhibition of ER-Golgi trafficking by treatment with the dihydropyridine FLI-06 (1 μ M)²⁷ diminished the effect of CSNK2B inhibition on ERSE promoter activity (Figure 2H).

The ATF6 α Branch of the UPR is a Critical Modulator of ER-Stress-Induced Proinflammatory Signals in IECs

Unresolved ER stress in IECs has emerged as an important mechanism favoring intestinal inflammation.⁸ First, we examined the levels of proinflammatory cytokines in intestinal organoids derived from Atf6tgtg transgenic mice and littermate control mice. Atf6tgtg organoids displayed an elevation of transcript levels of *Cxcl1* and *Tnf α* in the presence of tunicamycin, confirming a co-activating role of nATF6 α (Figure 3A). Levels of the ER stress target gene transcripts (*Hspa5* and *Hsp90b1*) as well as the ATF6 transcript itself could also be synergistically increased by tunicamycin stimulation in Atf6tgtg transgenic organoids. We detected, both on mRNA and on protein level, altered expression of canonical and noncanonical NF- κ B signaling components, indicated by increased levels of *Rela* and p-p65

Figure 3. ATF6 α regulates NF- κ B signaling on ER-stress induction. (A) *Cxcl1*, *Tnf α* , *Hspa5* (*Grp78*), *Hsp90b1* (*Grp94*), *Atf6* transcript levels of in WT and *Atf6 α* transgenic (Atf6 tgtg) SI organoids stimulated with tunicamycin (100 ng/mL, 24 hours). (B) *Cxcl1* and *Tnf α* mRNA levels in WT and Atf6 tgtg SI organoids stimulated for 24 hours. (C and D) NF- κ B promoter activity in Caco-2 cells on (C) inhibition of S1P with PF-429242 (10 μ M) or (D) siRNA-mediated depletion of ATF6 α (siATF6), ACSL1 (siACSL1), or CSNK2B (siCSNK2B). (E) NF- κ B dual luciferase reporter assay in Caco-2 cells stimulated with lipofectamine-complexed Palmitoyl coenzyme A (100 μ M) or lipofectamine alone (Lipo) for 24 hours. Depicted data representative of 3 independent experiments. Statistical analysis was performed using one-way analysis of variance together with post hoc Tukey test.



levels and increased levels of *Relb*, *Nfkb2*, p100, and p52, respectively (Supplementary Figure 2B and C) already at baseline. This was accompanied by enhanced phosphorylation of p38 (Supplementary Figure 2C) in the Atf6tggtg organoids. In line with these findings, inhibition of NF- κ B signaling using the aromatic diamine JSH-23, which blocks the nuclear translocation of NF- κ B,²⁸ abolished the proinflammatory signature in organoids overexpressing the N-terminal ATF6 fragment illustrated by significantly reduced mRNA levels of both *Cxcl1* and *Tnf α* upon ER-stress induction (Figure 3B). As ER-stress dependent activation of proinflammatory signals might involve autocrine release of TNF α ,⁵ we employed an anti-TNF neutralizing antibody (100 ng/mL) in Atf6tggtg organoids, which, however, only had mild effects on the mRNA levels of these proinflammatory cytokines and 2 NF- κ B target genes (*Birc2/3*)²⁹ (Figure 3B, Supplementary Figure 2D). Of note, whereas it has been shown that a ENU-induced hypomorphic mutation of the S1P gene renders mice susceptible to colitis,³⁰ pharmacological inhibition of S1P required for ATF6 α cleavage at the Golgi complex with PF-429242 (10 μ M) was able to inhibit tunicamycin-induced NF- κ B reporter activation (Figure 3C). To further validate this finding, we performed siRNA knockdown of ATF6 α , *ACSL1*, or *CSNK2B* in IECs and could confirm the co-activation effect of the endogenous ATF6 signaling module on NF- κ B reporter gene activity on ER-stress induction (Figure 3D). In agreement with these findings, stimulation with the ACSL1 product Palmitoyl coenzyme A caused increased NF- κ B reporter gene activity (Figure 3E). Taken together, our results identify ATF6 as a critical regulator of proinflammatory signaling in IECs and suggests a functional interaction of NF- κ B and ATF6 signaling under conditions of ER stress.

Inhibition of the ATF6 α Activators CSNK2B and ACSL1 Attenuates the Proinflammatory Profile of Genetically Induced ER stress: Impact of ATF6 α Signaling on *Xbp1*- and *Atg16l1*-deficiency

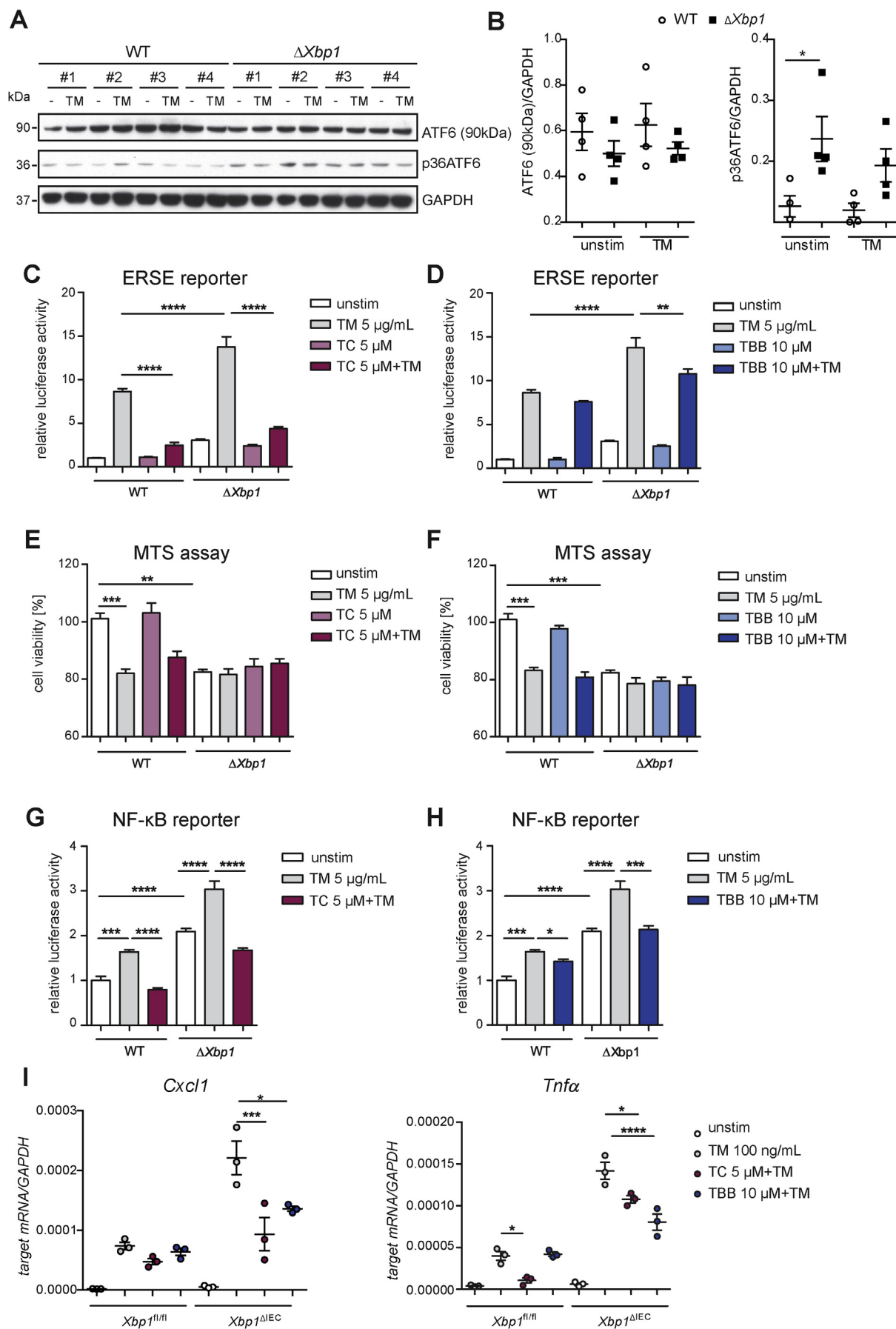
We next turned our attention to a potential role of ATF6 α and its upstream regulators for the execution of impaired, proinflammatory ER-stress responses observed in *Xbp1*- and *Atg16l1*-deficient IECs.^{5,8,13,14} Indeed, *Caco-2* cells carrying a genetic deletion of the autophagy gene *ATG16L1* introduced by CRISPR-Cas9¹⁴ (Δ ATG16L1-*Caco-2*) exhibited increased ATF6 α cleavage compared to their respective WT

comparators (WT-*Caco-2*) (Figure 4A and B). In addition, the ERSE reporter assays revealed significantly increased activation of the ATF6 α branch in Δ ATG16L1 cells compared with WT (Figure 4C), both at baseline and on further ER-stress induction with tunicamycin (5 μ g/mL). Likewise, *Atg16l1*-deficient SI organoids showed an up-regulation of ATF6 target genes compared with WT controls (Supplementary Figure 3A). Tunicamycin-induced ERSE reporter activity and target gene induction could be blocked by the cognate inhibitors TC (ACSL1) or TBB (CSNK2B), respectively (Figure 4C and D). In addition, cell viability of Δ ATG16L1 cells on ER-stress induction-assessed by MTS assay was significantly improved by treatment with the 2 ATF6 inhibitors (Figure 4E and F). Next, we sought to study the effect of inhibition of the ATF6 α branch on the increased NF- κ B signaling tone in autophagy-deficient IECs.³¹ Δ ATG16L1-*Caco2* cells transfected with an NF- κ B reporter plasmid showed increased activity upon tunicamycin stimulation compared with WT cells (Figure 4G and H). Notably, treatment with TBB/TC again significantly reduced NF- κ B reporter gene activity. Increased mRNA levels of *Cxcl1* and *Tnf α* observed in the *Atg16l1*-deficient organoids were reduced on treatment with the ACSL1 and the CSNK2B inhibitor, respectively (Figure 4I).

We also found elevated activation of the ATF6 α arm in the SI epithelial cell line MODE-K stably transduced with a short hairpin *Xbp1* (*shXbp1*) lentiviral vector (Figure 5A-C, Supplementary Figure 3C).⁵ We detected enhanced mRNA levels of ATF6 α targets (*Hsp90b1*, *Hspa5*) in *Xbp1*-deficient SI organoids (Supplementary Figure 3B). Inhibition of ATF6 α signaling by treatment with TC or TBB alleviated ERSE promoter activity (Figure 5C and D) and improved cell viability on ER-stress induction in MODE-K.i*Xbp1* (Δ *Xbp1*) cells (Figure 5E and F). Moreover, both augmented NF- κ B activity (Figure 5G and H) in Δ *Xbp1* cells, and *Cxcl1* and *Tnf α* levels in *Xbp1*-deficient organoids (Figure 5I) were reduced in the presence of the inhibitors on tunicamycin treatment compared with controls.

We next assessed the contribution of ATF6 α signaling to the ileitis phenotype of *Atg16l1* ^{Δ IEC} mice in a short-term (24 hours, Supplementary Figure 4) and in a longer in vivo ER stress model, in which mice were followed up for 72 hours (Figure 6). In both experiments, *Atg16l1*^{fl/fl} and *Atg16l1* ^{Δ IEC} mice were injected IP with a single dose of tunicamycin (1 mg/kg body weight) at 0 hour. To block ATF6 α -mediated signaling, mice were simultaneously injected with either TC

Figure 4. Reduction of the hyperactivation of the ATF6 α branch in *ATG16L1*-deficient IECs alleviates levels of proinflammatory cytokines. (A) Western blot analysis and quantification (B) of Δ ATG16L1-*Caco-2* and the WT cells. Cells stimulated with tunicamycin (5 μ g/mL, 6 hours). #1 to #4 refers to 4 independent biological replicates derived from one CRISPR clone. (C) Effects of TC and (D) TBB on the ERSE promoter in *Caco-2* cells measured by dual luciferase reporter assays. Cell viability of *Caco-2* WT and Δ ATG16L1-deficient cells quantified by MTS assay in the presence of TC (E) and TBB (F) after tunicamycin stimulation (5 μ g/mL, 24 hours). (G-H) NF- κ B Luciferase activity in *Caco-2* WT and *ATG16L1*-deficient cells. Cells stimulated with tunicamycin (5 μ g/mL, 24 hours) in the presence or absence of (G) TC (5 μ M) or (H) TBB (10 μ M). (I) *Cxcl1* and *Tnf α* transcript levels in SI organoids (*Atg16l1*^{fl/fl}, *Atg16l1* ^{Δ IEC}) treated with tunicamycin (100 ng/mL) and TC/TBB (24 hours, n = 3). Shown data representative of 3 independent experiments. Statistical analysis was performed using 1-way analysis of variance together with Tukey post hoc test.



or CX-4945 (silmatasertib) at 0 hour, and in addition at 24 hours, and 48 hours post tunicamycin injection in case of the 72-hour experiment (see Figure 6A and Supplementary Figure 5A for experimental design). Similar to TBB, CX-4945 is an ATP-competitive inhibitor of the CK2 and inhibited ATF6-mediated ERSE and NF- κ B reporter gene activity in Δ ATG16L1-Caco-2 cells (Supplementary Figure 3D and E). However, superior to TBB, CX-4945 is orally bioavailable³² and is currently tested in clinical trials for hematological and solid cancer treatment (ClinicalTrials.gov NCT01199718, NCT02128282, NCT00891280). Both TC and CX-4945 injections significantly attenuated tunicamycin-mediated body weight loss after 72 hours in *Atg16l1* ^{Δ IEC} mice (Figure 6B, Supplementary Figure 5A). Moreover, we observed attenuated shortening of the small intestine (Figure 6C), reduced Cxcl1 protein levels in the serum (Figure 6D) of *Atg16l1* ^{Δ IEC} mice, and reduced mRNA levels of *Tnf α* and *Ifit1* on tunicamycin injection in the presence of the tested inhibitors (Supplementary Figure 5B and C). Both transcripts are known to be induced by ER stress signals in *Atg16l1* ^{Δ IEC} mice.¹⁴ Likewise, histological analysis demonstrated reduced levels of inflammation (Figure 6G) and reduced epithelial cell death as depicted by reduced numbers of TUNEL⁺ epithelial cells in *Atg16l1*-deficient IECs in the presence of the tested inhibitors (Figure 6E and F). Staining was concentrated at the bottom of the crypts and, in line with previous studies, marked Paneth cells as well as other epithelial cells.^{14,33} In line with these findings, already 24 hours after tunicamycin injection, TC and CX-4945 treatment resulted in reduced epithelial cell death in the absence of *Atg16l1* as assessed by TUNEL staining (Supplementary Figure 4D and E), and reduced mRNA levels of *Tnf α* and *Ifit1* (Supplementary Figure 4F).

Limiting ATF6 α Signaling Attenuates the Proinflammatory Profile in Human Organoids on ER-stress Induction: Relevance for Human IBD

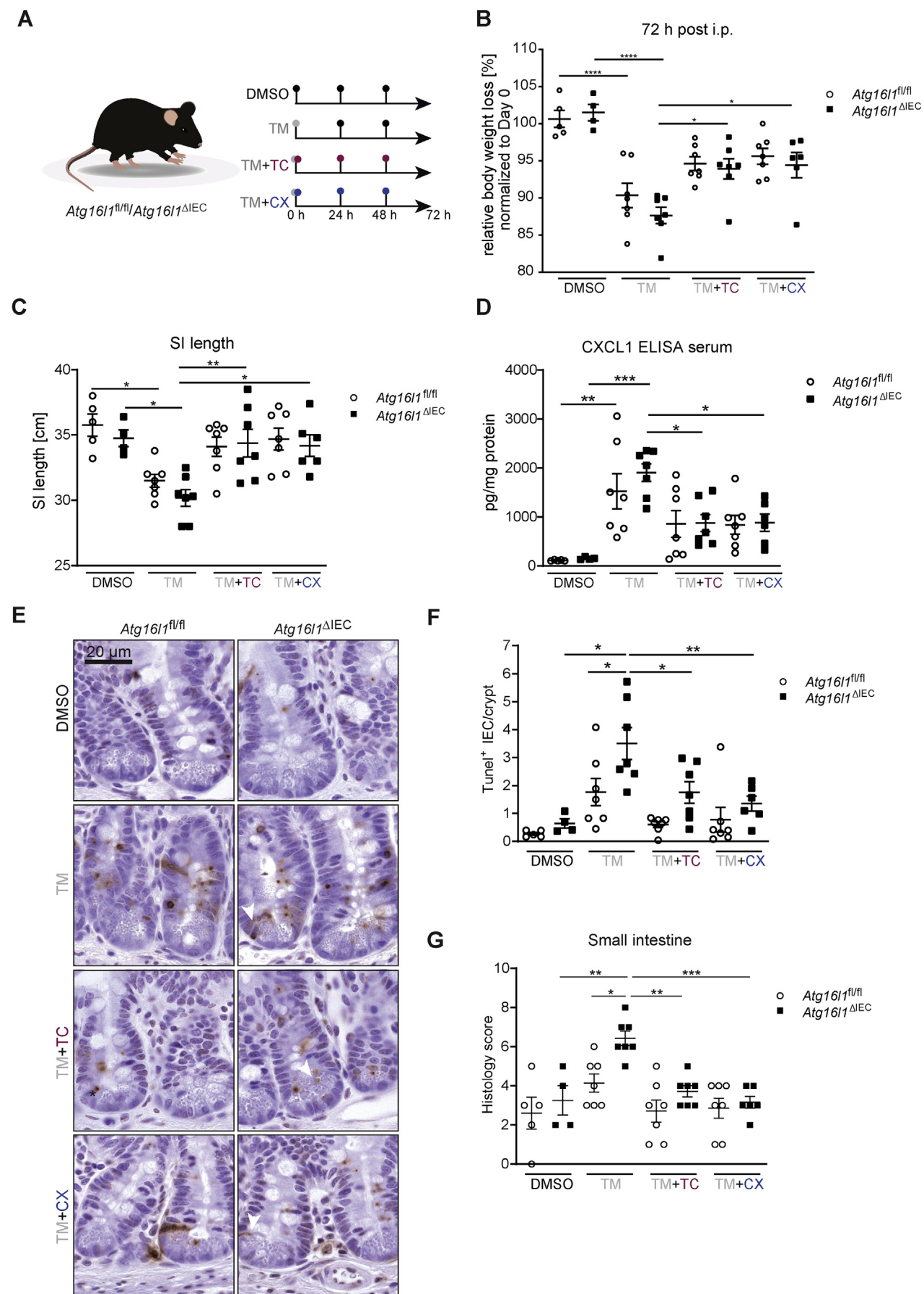
We next assessed expression levels and activation of ATF6 in human patients with IBD. Analysis of mRNA level in purified IECs from ileal biopsies revealed significantly higher expression of ATF6 α and the ATF6 target *HSPA5* in pediatric patients with CD compared with healthy controls (Figure 7A, comparison with ulcerative colitis in Supplementary Figure 6B).³⁴ Likewise, *CSNK2B*, but not *ACSL1* mRNA levels were upregulated (Supplementary

Figure 6B). Using protein lysates of early-passage ileal human organoids from patients with CD and healthy controls, we next demonstrated higher levels of the active p36 fragment of ATF6 α in organoids derived from adult patients with CD, which was more pronounced in organoids from inflamed tissue (Figure 7B, Supplementary Figure 6A, Supplementary Table 2). Next, we analyzed mRNA levels of ATF6 targets in human organoids generated from biopsies of patients with CD and healthy controls. On tunicamycin-mediated ER stress induction, we detected significantly increased levels of *HSPA5*, *DNAJC3*, and *HSP90B1* in organoids derived from patients with CD compared with healthy controls (Figure 7C). Subsequently, we investigated in human ileal organoids whether ATF6 α signaling can be limited by ACSL1- or CSNK2B inhibition. Indeed, exposure to either TC (Figure 7D) or TBB (Figure 7E) resulted in significantly reduced expression of ATF6 α targets on exposure to tunicamycin. Importantly, inhibition of ATF6 α signaling by TC or TBB, respectively, resulted in significantly lower mRNA expression of proinflammatory cytokines (*IL8*, *TNF α*) in human organoids exposed to tunicamycin (Figure 7F and G).

Discussion

In this study, we identified regulators of ATF6 α signaling using a stringent siRNA screening approach. Among the 22 validated upstream regulators of ATF6 α , *ACSL1* and *CSNK2B* were further analyzed. ACSL1 (acyl-CoA synthetase long chain family member 1) is a 78-kDa intrinsic membrane protein that mediates the conversion of fatty acids to acyl-CoAs. Importantly, ACSL1 localizes to the ER and to mitochondria-associated membranes. The other identified ATF6 α co-activator *CSNK2B* encodes the regulatory subunit of the CK2, which is a tetrameric serine/threonine-selective protein kinase composed of 2 catalytic subunits and 2 regulatory subunits. CK2 is localized in the ER and the Golgi complex.³⁵ Several studies have described a modulatory function of the CK2 on the UPR.^{36,37} However, to our knowledge, none of these studies have provided a mechanistic link between the ATF6 α branch of the UPR and CSNK2B. Using transgenic organoids overexpressing a constitutively active ATF6 α form, which mimics the S1P-cleaved protein, we show that the 2 targets act either downstream (ACSL1) or upstream (CK2) of the cleavage event. It is important to note that pharmacological inhibition of the upstream ATF6 α regulators did not completely

Figure 5. Inhibition of the ATF6 α branch in *Xbp1*-deficient IECs alleviates levels of proinflammatory cytokines. (A) Immunoblotting and quantification (B) of MODE-K cells stably transduced with a short hairpin *Xbp1* lentiviral vector and the respective WT control. Cells stimulated with tunicamycin (5 μ g/mL, 6 hours). #1 to #4 refers to 4 independent biological replicates. (C and D) Activation of the ATF6 α branch upon ER-stress induction (tunicamycin, 24 h, 5 μ g/mL) quantified in the presence of (C) TC and (D) TBB in MODE-K.*Xbp1* (Δ *Xbp1*) and MODE-K.*iCtrl* (WT) cells by dual luciferase reporter assays. Effects of TC (E) and TBB (F) on cell viability quantified by MTS assay after exposure to tunicamycin (5 μ g/mL, 24 hours) in WT and Δ *Xbp1* cells. (G and H) NF- κ B luciferase activity in WT and *Xbp1*-deficient Mode-K cells. Cells exposed to tunicamycin (5 μ g/mL, 24 hours) in the presence or absence of (G) TC (5 μ M) or (H) TBB (10 μ M). (I) Quantitative PCR of *Cxcl1* and *Tnf α* of SI organoids (*Xbp1*^{fl/fl}, *Xbp1* ^{Δ IEC}) treated with tunicamycin (100 ng/mL) and inhibitors (TC 5 μ M; TBB 10 μ M) for 24 hours (n = 3). Data shown are representative of 3 independent experiments. For statistical analysis, 1-way analysis of variance together with Tukey post hoc test was performed.



abolish all tunicamycin-mediated ER stress effects. This could be due to incomplete abrogation of ATF6 α signals by the inhibitors, but also due to the extensive crosstalk between the 3 UPR branches,^{1,38} which should be carefully considered when targeting the UPR for therapeutic benefit.

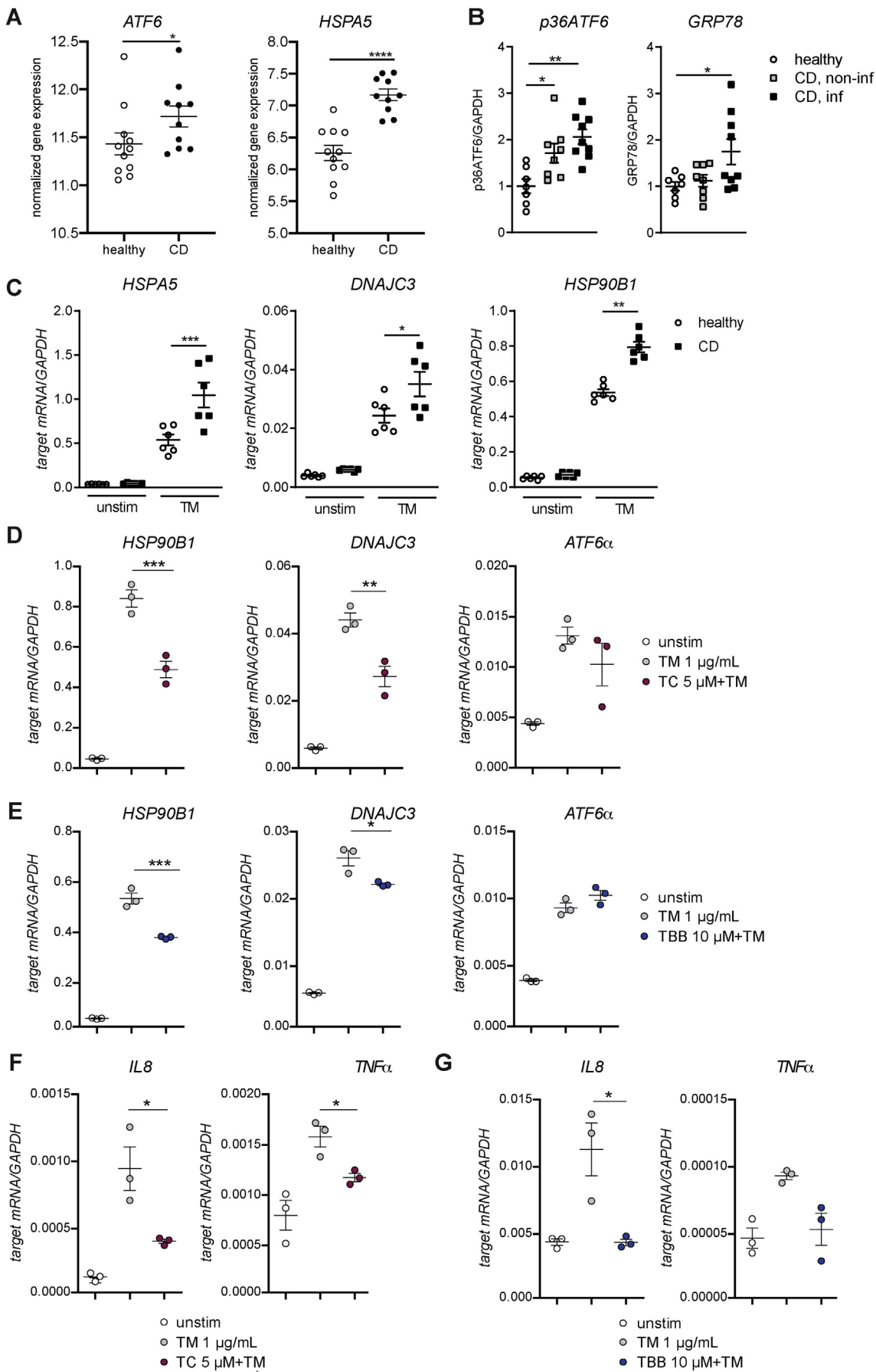
Several studies have revealed an intensive crosstalk between unresolved ER stress, failing autophagy and proinflammatory signaling in IECs in the context of IBD.^{5,8,13,14,39} In *Xbp1*- and *Atg16l1*-deficient IECs, increased TNF-dependent NF- κ B signaling and spontaneous intestinal inflammation *in vivo* are observed and have been attributed to elevated IRE1 α levels.^{5,8,13} In this context, our study reveals a significantly increased activation of the ATF6 α branch in cells lacking the autophagy gene *Atg16l1* or the UPR gene *Xbp1*. Importantly, inhibition of ATF6 α upstream signaling using the small molecule inhibitors TC/TBB was able to diminish the observed hyperinflammatory phenotype of *Atg16l1*- and *Xbp1*-deficient cells.^{5,13} Interestingly, direct activation of ATF6 α by active IRE1 has been proposed⁴⁰ and our data suggest a role of ATF6 α and its upstream regulators for the execution of impaired, proinflammatory ER-stress responses in IECs. It has been proposed that ATF6 α induces the phosphorylation of AKT to finally activate NF- κ B signaling,^{41,42} but engagement of other proinflammatory signaling events (eg, the activation of p38MAPK) have also been reported during ER stress.⁴³ As MAPK activation has been shown to shift the balance of NF- κ B signals in IECs from an antiapoptotic to a proinflammatory function,⁴⁴ such additional signals could be important for the effector function of ATF6 itself or might be modulated by downstream effectors of ATF6 α .

In line with a co-activating role of ATF6 on the NF- κ B pathway, we demonstrate an up-regulation of components of the NF- κ B machinery (*NF- κ B2* coding for p100 and its processed form p52) and increased p65 as well as p38MAPK phosphorylation in organoids overexpressing the active N-terminal ATF6 α fragment already under steady-state conditions. It must be noted that this model only incompletely reflects the physiological situation of normal ATF6 activation as the organoids face a constant stimulation by the transgene-encoded transcription factor; however under additional stimulation with the ER stress inducer tunicamycin, synergistic induction of *Cxcl1* and *Tnfa* mRNA levels was still observed. The induction of the 2 transcripts could be blocked by an inhibitor of the nuclear translocation of p65,²⁸ whereas it was only partially inhibited by application of anti-TNF antibodies arguing against a main role of autocrine TNF release in this system.

We have shown that homozygous *Atf6*tggtg mice develop spontaneous colon adenomas at 12 weeks of age.²⁴ Increased proinflammatory cytokine mRNA levels in this model were only detected at late stages of tumor development in whole colon tissue (>20 weeks) supporting the hypothesis that ATF6 α activation alone is not sufficient to generate IBD-like tissue pathology, but additional signals must be present. As tunicamycin inhibits N-linked protein glycosylation and thereby activates additional ER stress signaling at the level of all 3 UPR branches,⁴⁵ which includes IRE1-dependent signaling, the results suggest that the ATF6 α branch serves as a co-activating executioner toward a hyperinflammatory phenotype. Pharmacological inhibition of the 2 ATF6 α upstream activators CSNK2B and ASCL1 on tunicamycin application *in vivo* was able to block ER stress-induced epithelial cell death and signs of mucosal inflammation in the SI. The protective effect was more pronounced in mice lacking *Atg16l1* in the intestinal epithelium, which are prone to develop ileal inflammation dependent on IRE1 and the TNFR1-NF- κ B axis,^{5,13} and to TNF-dependent necroptosis.³³ Still, it remains an interesting question whether and how ATF6 α acts upon the autophagic flux of IECs under autophagy-proficient conditions.

These observations in the SI are important for human IBD, as the role of ATF6 α signaling in intestinal inflammation has only been shown in colonic IECs from patients with ulcerative colitis, where increased cleavage of ATF6 α and augmented expression of the ATF6 α targets *GRP78* and *GRP94* were demonstrated.¹² Increased ATF6 α expression itself was recently suggested as a marker for precancerous dysplasia in colitis-associated colorectal cancer.⁴⁶ Here, we show that increased mRNA levels and activation of the ATF6 branch are present in SI epithelial cells from patients with CD. This activatability is maintained, at least during early passages, in patient-derived small intestinal organoids, arguing for a sustained deregulation of this pathway in this disease condition. It is important to note that, although the hypomorphic *ATG16L1*^{T300A} variant is a risk factor for ileal CD,⁴⁷ it seems unlikely that small intestinal ATF6 hyperactivation can be explained by genetics only. ER stress rather should be regarded as a central hub integrating signals on the state of the cell.⁴⁸ As such it is influenced by a variety of environmental factors, such as diet,⁴⁹ microbiota,⁵⁰ or proliferative signals^{14,51} that act on IECs as a barrier constituent. The individual life history of exposure to such stressors may exceed the epithelium's resilience leading to unresolved ER stress and ATF6 activation as a proinflammatory signal, whereby

Figure 6. Inhibition of the ATF6 α branch mitigates ER-stress mediated inflammation and cell death in *Atg16l1*^{ΔIEC} mice. (A) Stimulation scheme of *Atg16l1*^{fl/fl} and *Atg16l1*^{ΔIEC} mice (*n* = 4–7). Mice were treated with 1 mg/kg bodyweight of tunicamycin IP, when indicated mice additionally received either TC (2.5 μg/g bodyweight) or CX-4945 (40 μg/g body weight) at 0, 24, and 48 hours. Control groups received dimethyl sulfoxide. After 72 hours mice were killed. (B) Weight loss 72 hours after injection. (C) SI length 72 hours after injection. (D) CXCL1 concentration in serum quantified by enzyme-linked immunosorbent assay. (E and F) TUNEL staining of SI sections with representative pictures (E, arrowheads denote TUNEL+ IECs outside of the Paneth cell/stem cell niche) and quantification (F). Bars = 20 μm. A minimum of 50 crypts/intestine were assessed in each treatment group. (G) Histological evaluation of small intestinal sections. Statistical analysis was performed using 1-way analysis of variance together with Tukey post hoc test.



hypomorphic ATG16L1^{T300A} may be an important determinant of the threshold.

Our findings suggest that engagement of the ATF6 α branch may represent an executioner mechanism of proinflammatory ER stress signals, particularly in IECs with defective autophagy or exaggerated UPR signaling. We demonstrate the presence of activated ATF6 signaling as a characteristic feature of small intestinal IECs isolated from patients with CD. Importantly, we show that inhibition of the ATF6 branch is able to mitigate the proinflammatory signature of ER stress induction in human small intestinal organoids. Interfering with the ATF6 α pathway targeting the upstream inducers ACSL1 and CSNK2B, respectively, might thus represent a novel therapeutic approach in intestinal inflammation.

Supplementary Material

Note: To access the supplementary material accompanying this article, visit the online version of *Gastroenterology* at www.gastrojournal.org, and at <https://doi.org/10.1053/j.gastro.2020.06.088>.

References

- Grootjans J, Kaser A, Kaufman RJ, et al. The unfolded protein response in immunity and inflammation. *Nat Rev Immunol* 2016;16:469–484.
- Haze K, Yoshida H, Yanagi H, et al. Mammalian transcription factor ATF6 is synthesized as a transmembrane protein and activated by proteolysis in response to endoplasmic reticulum stress. *Mol Biol Cell* 1999;10:3787–3799.
- Harding HP, Zhang Y, Ron D. Protein translation and folding are coupled by an endoplasmic-reticulum-resident kinase. *Nature* 1999;397:271–274.
- Yoshida H, Haze K, Yanagi H, et al. Identification of the cis-acting endoplasmic reticulum stress response element responsible for transcriptional induction of mammalian glucose-regulated proteins. Involvement of basic leucine zipper transcription factors. *J Biol Chem* 1998;273:33741–33749.
- Adolph TE, Tomczak MF, Niederreiter L, et al. Paneth cells as a site of origin for intestinal inflammation. *Nature* 2013;503:272–276.
- Bernales S, McDonald KL, Walter P. Autophagy counterbalances endoplasmic reticulum expansion during the unfolded protein response. *PLoS Biol* 2006;4:e423.
- Deuring JJ, Fuhler GM, Konstantinov SR, et al. Genomic ATG16L1 risk allele-restricted Paneth cell ER stress in quiescent Crohn's disease. *Gut* 2014;63:1081–1091.
- Kaser A, Lee AH, Franke A, et al. XBP1 links ER stress to intestinal inflammation and confers genetic risk for human inflammatory bowel disease. *Cell* 2008;134:743–756.
- Ogata M, Hino S, Saito A, et al. Autophagy is activated for cell survival after endoplasmic reticulum stress. *Mol Cell Biol* 2006;26:9220–9231.
- Heazlewood CK, Cook MC, Eri R, et al. Aberrant mucin assembly in mice causes endoplasmic reticulum stress and spontaneous inflammation resembling ulcerative colitis. *PLoS Med* 2008;5:e54.
- Shkoda A, Ruiz PA, Daniel H, et al. Interleukin-10 blocked endoplasmic reticulum stress in intestinal epithelial cells: impact on chronic inflammation. *Gastroenterology* 2007;132:190–207.
- Treton X, Pedruzzi E, Cazals-Hatem D, et al. Altered endoplasmic reticulum stress affects translation in inactive colon tissue from patients with ulcerative colitis. *Gastroenterology* 2011;141:1024–1035.
- Tschurtschenthaler M, Adolph TE, Ashcroft JW, et al. Defective ATG16L1-mediated removal of IRE1 α drives Crohn's disease-like ileitis. *J Exp Med* 2017;214:401–422.
- Aden K, Tran F, Ito G, et al. ATG16L1 orchestrates interleukin-22 signaling in the intestinal epithelium via cGAS-STING. *J Exp Med* 2018;215:2868–2886.
- Wu J, Rutkowski DT, Dubois M, et al. ATF6 α optimizes long-term endoplasmic reticulum function to protect cells from chronic stress. *Dev Cell* 2007;13:351–364.
- Yamamoto K, Sato T, Matsui T, et al. Transcriptional induction of mammalian ER quality control proteins is mediated by single or combined action of ATF6 α and XBP1. *Dev Cell* 2007;13:365–376.
- Sato T, Vries RG, Snippert HJ, et al. Single Lgr5 stem cells build crypt-villus structures in vitro without a mesenchymal niche. *Nature* 2009;459:262–265.
- Fujii S, Suzuki K, Kawamoto A, et al. PGE2 is a direct and robust mediator of anion/fluid secretion by human intestinal epithelial cells. *Sci Rep* 2016;6:36795.
- Lipinski S, Grabe N, Jacobs G, et al. RNAi screening identifies mediators of NOD2 signaling: implications for

Figure 7. Limiting ATF6 α signaling attenuates ER-stress mediated inflammation in human organoids. (A) Relative mRNA expression of ATF6 α and HSPA5 in IECs from ileal biopsies from pediatric patients with CD and healthy controls. (B) Quantification of protein levels of p36ATF6 and GRP78 derived from SI organoid lysates generated from healthy, CD non-inflamed, and CD inflamed tissue, respectively. (C) mRNA levels of HSPA5, DNAJC3, and HSP90B1 in human SI organoids from healthy controls and patients with CD treated with tunicamycin (1 μ g/mL; 24 hours). (D) Transcript levels of HSP90B1 and DNAJC3 in human SI organoids treated with tunicamycin (1 μ g/mL) and TC (D) or TBB (E) for 24 hours. (F and G) IL8 and TNF α transcript levels in human SI organoids treated with tunicamycin (1 μ g/mL) and inhibitor TC (F) or TBB (G), respectively (24 hours, n = 3). Depicted data representative of 3 independent experiments. Each data point represents 1 organoid line derived from an individual patient with CD. Statistical analysis was performed using 1-way analysis of variance together with Tukey post hoc test or Mann-Whitney test (for pair comparisons).

- spatial specificity of MDP recognition. *Proc Natl Acad Sci U S A* 2012;109:21426–21431.
20. Livak KJ, Schmittgen TD. Analysis of relative gene expression data using real-time quantitative PCR and the 2(-Delta Delta C(T)) Method. *Methods* 2001;25:402–408.
 21. Smidt K, Jessen N, Petersen AB, et al. SLC30A3 responds to glucose- and zinc variations in beta-cells and is critical for insulin production and in vivo glucose-metabolism during beta-cell stress. *PLoS One* 2009;4:e5684.
 22. Schwab ME. Functions of Nogo proteins and their receptors in the nervous system. *Nat Rev Neurosci* 2010;11:799–811.
 23. Dixon SJ, Lemberg KM, Lamprecht MR, et al. Ferroptosis: an iron-dependent form of nonapoptotic cell death. *Cell* 2012;149:1060–1072.
 24. Coleman OI, Lobner EM, Bierwirth S, et al. Activated ATF6 induces intestinal dysbiosis and innate immune response to promote colorectal tumorigenesis. *Gastroenterology* 2018;155:1539–1552.
 25. Koreishi M, Yu S, Oda M, et al. CK2 phosphorylates Sec31 and regulates ER-To-Golgi trafficking. *PLoS One* 2013;8:e54382.
 26. Schindler AJ, Schekman R. In vitro reconstitution of ER-stress induced ATF6 transport in COPII vesicles. *Proc Natl Acad Sci U S A* 2009;106:17775–17780.
 27. Kramer A, Mentrup T, Kleizen B, et al. Small molecules intercept Notch signaling and the early secretory pathway. *Nat Chem Biol* 2013;9:731–738.
 28. Shin HM, Kim MH, Kim BH, et al. Inhibitory action of novel aromatic diamine compound on lipopolysaccharide-induced nuclear translocation of NF-kappaB without affecting IkappaB degradation. *FEBS Lett* 2004;571:50–54.
 29. Till A, Rosenstiel P, Krippner-Heidenreich A, et al. The Met-196 -> Arg variation of human tumor necrosis factor receptor 2 (TNFR2) affects TNF-alpha-induced apoptosis by impaired NF-kappaB signaling and target gene expression. *J Biol Chem* 2005;280:5994–6004.
 30. Brandl K, Rutschmann S, Li X, et al. Enhanced sensitivity to DSS colitis caused by a hypomorphic Mbtsp1 mutation disrupting the ATF6-driven unfolded protein response. *Proc Natl Acad Sci U S A* 2009;106:3300–3305.
 31. Liu T, Zhang L, Joo D, et al. NF-kappaB signaling in inflammation. *Signal Transduct Target Ther* 2017;2:17023.
 32. Siddiqui-Jain A, Drygin D, Streiner N, et al. CX-4945, an orally bioavailable selective inhibitor of protein kinase CK2, inhibits prosurvival and angiogenic signaling and exhibits antitumor efficacy. *Cancer Res* 2010;70:10288–10298.
 33. Matsuzawa-Ishimoto Y, Shono Y, Gomez LE, et al. Autophagy protein ATG16L1 prevents necroptosis in the intestinal epithelium. *J Exp Med* 2017;214:3687–3705.
 34. Howell KJ, Kraicz J, Nayak KM, et al. DNA methylation and transcription patterns in intestinal epithelial cells from pediatric patients with inflammatory bowel diseases differentiate disease subtypes and associate with outcome. *Gastroenterology* 2018;154:585–598.
 35. Faust M, Jung M, Gunther J, et al. Localization of individual subunits of protein kinase CK2 to the endoplasmic reticulum and to the Golgi apparatus. *Mol Cell Biochem* 2001;227:73–80.
 36. Hosoi T, Korematsu K, Horie N, et al. Inhibition of casein kinase 2 modulates XBP1-GRP78 arm of unfolded protein responses in cultured glial cells. *PLoS One* 2012;7:e40144.
 37. Manni S, Brancalion A, Tubi LQ, et al. Protein kinase CK2 protects multiple myeloma cells from ER stress-induced apoptosis and from the cytotoxic effect of HSP90 inhibition through regulation of the unfolded protein response. *Clin Cancer Res* 2012;18:1888–1900.
 38. Haze K, Okada T, Yoshida H, et al. Identification of the G13 (cAMP-response-element-binding protein-related protein) gene product related to activating transcription factor 6 as a transcriptional activator of the mammalian unfolded protein response. *Biochem J* 2001;355:19–28.
 39. Diamanti MA, Gupta J, Bennecke M, et al. IKKalpha controls ATG16L1 degradation to prevent ER stress during inflammation. *J Exp Med* 2017;214:423–437.
 40. Wang Y, Shen J, Arenzana N, et al. Activation of ATF6 and an ATF6 DNA binding site by the endoplasmic reticulum stress response. *J Biol Chem* 2000;275:27013–27020.
 41. Nakajima S, Hiramatsu N, Hayakawa K, et al. Selective abrogation of BiP/GRP78 blunts activation of NF-kappaB through the ATF6 branch of the UPR: involvement of C/EBPbeta and mTOR-dependent dephosphorylation of Akt. *Mol Cell Biol* 2011;31:1710–1718.
 42. Yamazaki H, Hiramatsu N, Hayakawa K, et al. Activation of the Akt-NF-kappaB pathway by subtilase cytotoxin through the ATF6 branch of the unfolded protein response. *J Immunol* 2009;183:1480–1487.
 43. Hung JH, Su IJ, Lei HY, et al. Endoplasmic reticulum stress stimulates the expression of cyclooxygenase-2 through activation of NF-kappaB and pp38 mitogen-activated protein kinase. *J Biol Chem* 2004;279:46384–46392.
 44. Guma M, Stepniak D, Shaked H, et al. Constitutive intestinal NF-kappaB does not trigger destructive inflammation unless accompanied by MAPK activation. *J Exp Med* 2011;208:1889–1900.
 45. Berger E, Haller D. Structure-function analysis of the tertiary bile acid TUDCA for the resolution of endoplasmic reticulum stress in intestinal epithelial cells. *Biochem Biophys Res Commun* 2011;409:610–615.
 46. Hanaoka M, Ishikawa T, Ishiguro M, et al. Expression of ATF6 as a marker of pre-cancerous atypical change in ulcerative colitis-associated colorectal cancer: a potential role in the management of dysplasia. *J Gastroenterol* 2018;53:631–641.
 47. Duraes C, Machado JC, Portela F, et al. Phenotype-genotype profiles in Crohn's disease predicted by

- genetic markers in autophagy-related genes (GOIA study II). *Inflamm Bowel Dis* 2013;19:230–239.
48. Hotamisligil GS. Endoplasmic reticulum stress and the inflammatory basis of metabolic disease. *Cell* 2010;140:900–917.
 49. Nezami BG, Mwangi SM, Lee JE, et al. MicroRNA 375 mediates palmitate-induced enteric neuronal damage and high-fat diet-induced delayed intestinal transit in mice. *Gastroenterology* 2014;146:473–483.e3.
 50. Hodin CM, Verdam FJ, Grootjans J, et al. Reduced Paneth cell antimicrobial protein levels correlate with activation of the unfolded protein response in the gut of obese individuals. *J Pathol* 2011;225:276–284.
 51. Powell N, Pantazi E, Pavlidis P, et al. Interleukin-22 orchestrates a pathological endoplasmic reticulum stress response transcriptional programme in colonic epithelial cells. *Gut* 2020;69:578–590.

Received August 29, 2019. Accepted June 18, 2020.

Correspondence

Address correspondence to: Philip Rosenstiel, MD, Institute of Clinical Molecular Biology, University Hospital Schleswig-Holstein, Campus Kiel; Rosalind-Franklin Str. 12 D-24105 Kiel, Germany. e-mail: p.rosenstiel@mucosa.de; fax: +49 (431) 500–12070.

CRedit Authorship Contributions

Stephanie T. Stengel, PhD (Data curation: Lead; Investigation: Lead; Methodology: Lead; Validation: Lead; Writing – original draft: Lead) Antonella Fazio, PhD (Formal analysis: Equal; Investigation: Supporting; Methodology: Supporting; Writing – review & editing: Supporting). Simone Lipinski, PhD (Formal analysis: Supporting; Investigation: Supporting; Methodology: Supporting; Writing – review & editing: Supporting). Martin T. Jahn, MSc (Data curation: Supporting; Formal analysis: Supporting; Investigation: Supporting). Konrad Aden, MD (Data curation: Supporting; Investigation: Supporting; Methodology: Supporting; Writing – review & editing: Supporting). Go Ito, MD (Formal analysis: Supporting; Methodology: Supporting; Writing – review & editing: Supporting). Felix Wottawa, MD student (Formal analysis: Supporting; Methodology: Supporting). Jan W.P.

Kuiper, PhD (Data curation: Supporting; Investigation: Supporting; Methodology: Supporting). Olivia I. Coleman, PhD (Methodology: Supporting; Resources: Supporting). Florian Tran, MD (Formal analysis: Supporting; Investigation: Supporting; Methodology: Supporting). Dora Bordoni, MSc (Investigation: Supporting; Methodology: Supporting). Joana P. Bernardes, PhD (Data curation: Supporting; Formal analysis: Supporting; Investigation: Supporting). Marlene Jentzsch, PhD (Investigation: Supporting; Methodology: Supporting). Anne Luzius, PhD (Investigation: Supporting; Methodology: Supporting). Sandra Bierwirth, MSc (Methodology: Supporting; Resources: Supporting). Berith Messner, MSc (Investigation: Supporting; Methodology: Supporting). Anna Henning, DVM (Investigation: Supporting; Methodology: Supporting). Lina Welz, MD student (Investigation: Supporting; Methodology: Supporting). Nassim Kakavand, MD student (Investigation: Supporting; Methodology: Supporting). Maren Falk-Paulsen, PhD (Investigation: Supporting; Methodology: Supporting; Supervision: Supporting). Simon Imm, MD student (Investigation: Supporting; Methodology: Supporting). Finn Hinrichsen, MD student (Formal analysis: Supporting; Methodology: Supporting; Writing – review & editing: Supporting). Matthias Zilbauer, MD (Data curation: Supporting; Formal analysis: Supporting; Writing – review & editing: Supporting). Stefan Schreiber, MD (Funding acquisition: Supporting; Validation: Supporting; Writing – review & editing: Supporting). Arthur Kaser, MD (Conceptualization: Supporting; Methodology: Supporting; Supervision: Supporting; Writing – review & editing: Supporting). Richard Blumberg, MD (Conceptualization: Supporting; Funding acquisition: Supporting; Investigation: Supporting; Resources: Supporting; Writing – review & editing: Supporting). Dirk Haller, PhD (Conceptualization: Supporting; Funding acquisition: Supporting; Supervision: Supporting; Writing – review & editing: Supporting). Philip C. Rosenstiel, MD (Conceptualization: Lead; Formal analysis: Supporting; Supervision: Lead; Writing – original draft: Equal; Writing – review & editing: Lead).

Conflict of interest

The authors disclose no conflicts.

Funding

This work was supported by DFG Excellence Clusters Inflammation at Interfaces and Precision Medicine in Inflammation (RTFII) (Philip Rosenstiel); the DFG Research Training Group 1743 (Philip Rosenstiel), the CRC877 B9 project (Philip Rosenstiel), H2020 SYSCID Contract 733100 (Philip Rosenstiel), the SH Excellence Chair program (Philip Rosenstiel); the Wellcome Trust Investigator award 106260/Z/14/Z (Arthur Kaser), European Research Council under the Horizon 2020 ERC CoG agreement no. 648889 (Arthur Kaser); Cambridge Biomedical Research Centre (Arthur Kaser) and the National Institutes of Health (grants DK044319, DK051362, DK053056, and DK088199) (Richard Blumberg) and grant to the Harvard Digestive Diseases Center DK034854 (Richard Blumberg). Dirk Haller is supported by the DFG CRC 1335 project P11. Support by the EU IMI2 grant 3TR (to S.S and P.R) is acknowledged.

Supplementary Material and Methods

Cell Culture and Reagents

Human embryonic kidney (HEK) 293 cells (ACC 305), and human colonic carcinoma Caco-2 (ACC 169) cells were purchased from the German Collection of Microorganisms and Cell Cultures (DSMZ, Braunschweig, Germany).

Camostat mesylate, FLI-06 and Simvastatin were purchased from Sigma-Aldrich (St Louis, MO). Erastin and TPEN were from Cayman (Ann Arbor, MI), TBB from Tocris (Bristol, UK), and CX-4945 from (Biomol, Hamburg, Germany). Triascin C was purchased from Enzo Life Sciences (Farmingdale, IL).

Cultivation of Murine SI Organoids

Crypts were isolated from mouse SI by EDTA-based Ca²⁺/Mg²⁺ chelation and intestinal organoids were cultivated as described by Sato et al.¹ In brief, SI was removed and cut longitudinally. Intestinal pieces were incubated in phosphate-buffered saline supplemented with 10 nM EDTA for 10 minutes intermittently by shaking. Supernatant was removed and phosphate-buffered saline-EDTA solution was added. This procedure was repeated 4 times. The crypt suspension was passed through a 100- μ m strainer and centrifuged at 400 g. Epithelial crypts were resuspended in Matrigel (BD Bioscience, San Jose, CA) and embedded in 24-well plates and cultivated in IntestiCult Organoid Growth Medium (STEMCELL; Vancouver, Canada). Medium was changed twice per week and organoids were stimulated after 7 days of cultivation. The mouse model for the SI organoids from Atf6tg and tg/wt and controls (Atf6 wt/wt) were described in Coleman et al.²

Culture of Human Intestinal Organoids

Human intestinal biopsy specimens were obtained from patients who underwent endoscopic examination. The study was approved by the Ethics Committee of the Medical Faculty, University Kiel (vote B231/98) and written informed consent was obtained from each patient before study-related procedures. Isolation of the crypts and establishment of intestinal organoids were performed as described.³ Briefly, crypts were collected by shaking biopsy specimens in 2.5 mM EDTA. Isolated crypts were embedded in Matrigel and placed in 24-well culture dish. Crypts were maintained in 50% L-WRN conditioned medium supplemented with recombinant human epidermal growth factor (50 ng/mL, PeproTech, Hamburg, Germany), Y-27632 (10 μ M, Sigma-Aldrich), A83-01 (500 nM, Tocris), Nicotinamide (10 mM, Sigma-Aldrich), N2 supplement and B12 supplement (Thermo Scientific) and SB202190 (10 μ M, Enzo); 50% L-WRN conditioned media was generated as previously described using the L-WRN cell line.⁴ Organoids were passaged every 6 to 7 days. For all experiments, organoids were used at passage 3 to 5.

Transfection of siRNA and Plasmid DNA

For reverse transfection of siRNA into cultured cells the polyamine-based transfection agent siPORT Amine (Life Technologies, Carlsbad, CA) was used according to the manufacturer's protocol. For transfection of plasmid DNA into cultured cells, FuGENE 6 (Promega, Madison, WI) was used according to the manufacturer's protocol.

High-throughput RNAi Screening Procedure

A total of 23,349 unique siRNAs targeting 7783 genes were screened using the Silencer Human Druggable Genome siRNA library V3 (Ambion, Austin, TX). HEK-293 cells were reverse transfected with either single siRNAs (Ambion; primary and secondary screen) or siRNA pools (siGENOME; SMARTpool; Dharmacon, Lafayette, LA; tertiary screen) complexed with siPORT Amine (Ambion).

Dual Luciferase Reporter Assays

Plasmid-encoded ERSE-dependent firefly luciferase (pGL3-ERSE, 12 ng/well) and a constitutive thymidine kinase driven *Renilla* luciferase were used in a dual luciferase assay (Clontech, 3 ng/well) to assay ATF6/ERSE activation. For quantification of the NF- κ B promoter activity, a reporter system based on NF- κ B responsive promoter elements driving expression of the Firefly luciferase (40 ng/well) was used.⁵ For all luciferase reporter assays, the fold change is depicted. For calculating the fold change, unstimulated WT controls were set to 1.

RNA Extracts and Quantitative Real-Time PCR

Total RNA was isolated using the RNeasy kit (Qiagen). Total RNA was reverse-transcribed to cDNA using the Maxima H Minus First Strand cDNA Synthesis kit (Thermo Scientific). Quantitative RealTime PCR was performed using the TaqMan Gene Expression Master Mix (Applied Biosystems) and analyzed by the 7900HT Fast Real Time PCR System (Applied Biosystems). The following TaqMan assays (Applied Biosystems) were used: *ACSL1*(00960561), *CSNK2B*(00365635), *ATF6*(00232586), *HSP90B1*(00427665), *DNAJC3*(00534483), *Hsp90b1*(00441926), *Hspa5*(00517690), and *Tnf*(00443258). Relative transcript levels were determined using the indicated housekeeper and the standard curve method.⁶

Immunoblotting

Cells were lysed in RIPA buffer (Thermo Scientific) in the presence of protease and phosphatase inhibitors. Precipitates were separated by SDS/PAGE. After transfer onto polyvinylidene fluoride membranes (Millipore, Burlington, MA), Western blots were performed as described.⁵ α -ATF6 antibody was purchased from Acris (SM7007P), α -GRP78 from Abcam (Cambridge, UK) (ab21685), α -ATG16L1 from CST (Danvers, MA) (#8089), GRP94 from CST (#2104), α -p100/p52 from CST (#52583), α -p-p65 from Abcam

(ab86299), α -p65 from CST (#82429, and α -p38 and α -p38 from CST (#9212 and #9211, respectively).

TUNEL Staining of Murine SI Tissue

Longitudinal ileal sections were fixed in 10% formalin. Sections of paraffin-embedded ileal Swiss rolls were deparaffinized with Tyrol substitute (Roth, Karlsruhe, Germany). Slides were subjected to Apop Tag Plus Peroxidase in situ Apoptosis Detection kit (Millipore). Slides were examined using a Zeiss (Jena, Germany) AxioImager.Z1 apotome microscope and AxioVision Rel 4.9 software.

Histopathological Analyses of Murine SI Tissue

Histological scoring was performed in a blinded fashion. The histological score displays the combined score of inflammatory cell infiltration and tissue damage as described elsewhere.⁷

Mice

Villin(*V*)-*cre*⁺; *Xbp1*^{fl/fl} (*Xbp1* ^{Δ IEC}),⁸ Villin(*V*)-*cre*⁺; *Atg16l1*^{fl/fl} (*Atg16l1* ^{Δ IEC})⁷ mice, backcrossed for at least 6 generations on a C57BL/6 background, were used at an age of 8 to 20 weeks. All mice were maintained in a specific pathogen-free facility. All experiments were performed in accordance with the guidelines for Animal Care of Kiel University and in conformity with national and international laws and policies and with appropriate permissions (acceptance no. V242-7224.121-33).

In Vivo Treatment of Mice

Atg16l1 ^{Δ IEC} or *Atg16l1*^{fl/fl} mice were treated with 1 mg/kg bodyweight tunicamycin or dimethyl sulfoxide IP for 24 or 72 hours before being killed. Groups of mice received 2.5 μ g/g bodyweight TC or 40 μ g/g bodyweight CX-4945 IP, respectively, at 0, 24, and 48 hours post Tunicamycin injection (72-hour experiment) or once at 0 hour (24-hour experiment). This animal experiment was approved by the Animal Investigation Committee of the University Hospital Schleswig-Holstein (acceptance no. V242-32647/2018 [59-7/18]).

Statistics

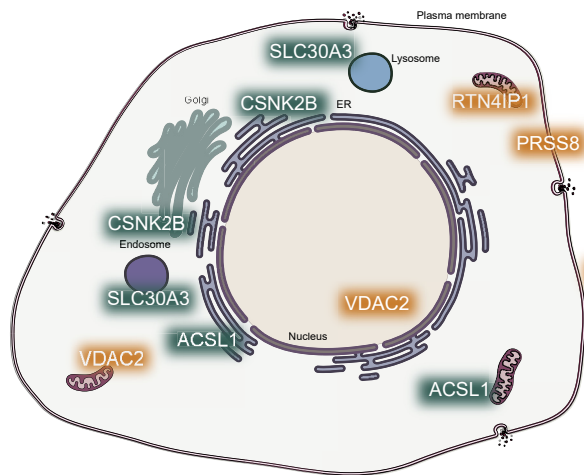
Statistical analysis was performed using the GraphPad Prism 5 software package (GraphPad Software Inc., La Jolla,

CA). Unless otherwise stated, the Student unpaired *t* test was performed. Data are shown as mean \pm standard error of the mean (SEM). In case multiple groups were compared, the analysis of variance with post hoc Tukey test was used for statistical analysis. A *P* value of $\leq .05$ was considered as significant (*). A *P* value of $\leq .01$ was considered as strongly significant (**) and *P* value of $\leq .001$ as highly significant (***). **** = *P* value $\leq .0001$.

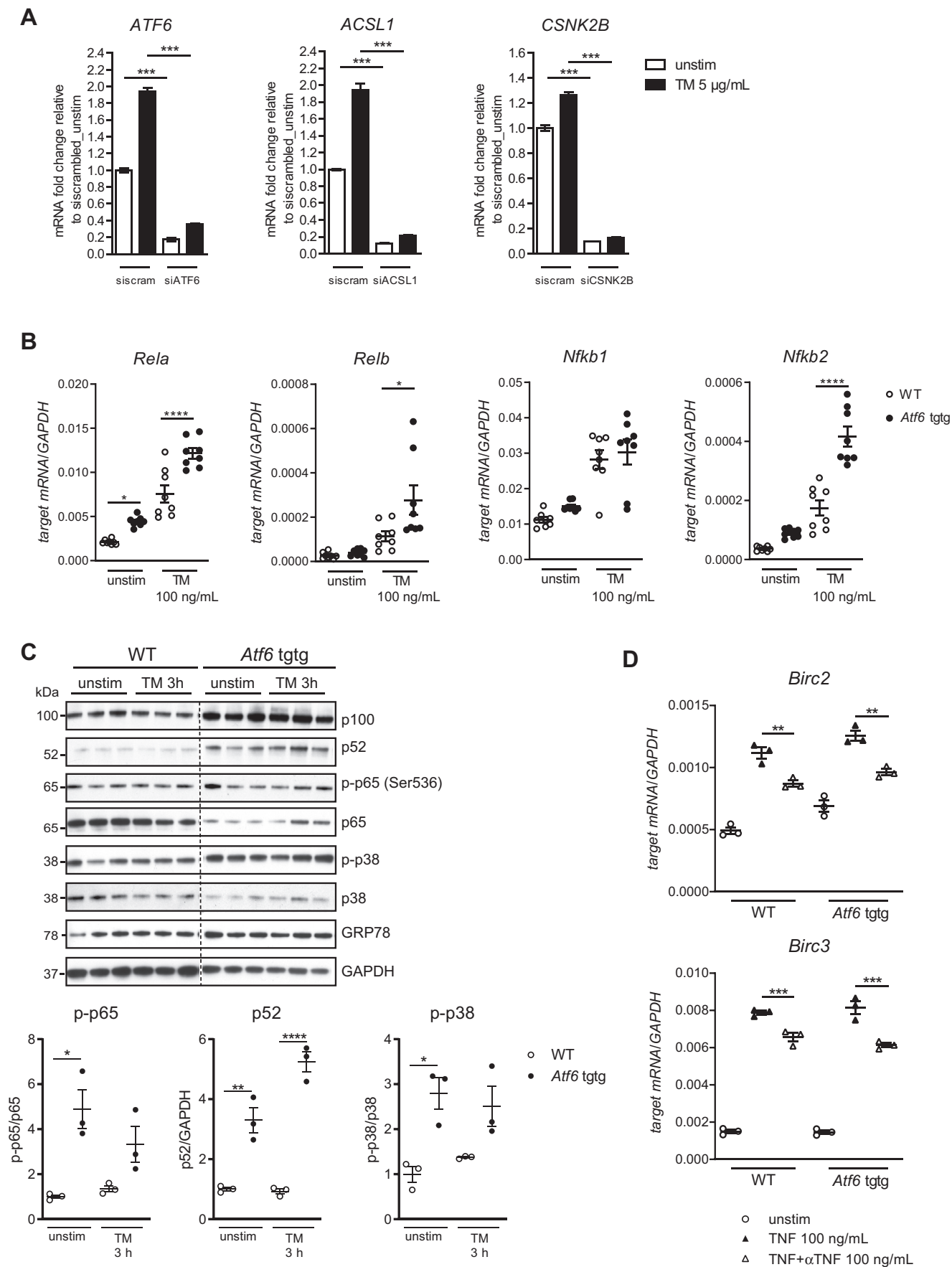
Supplementary References

1. Sato T, Vries RG, Snippert HJ, et al. Single Lgr5 stem cells build crypt-villus structures in vitro without a mesenchymal niche. *Nature* 2009;459:262-265.
2. Coleman OI, Lobner EM, Bierwirth S, et al. Activated ATF6 induces intestinal dysbiosis and innate immune response to promote colorectal tumorigenesis. *Gastroenterology* 2018;155:1539-1552.
3. Fujii S, Suzuki K, Kawamoto A, et al. PGE2 is a direct and robust mediator of anion/fluid secretion by human intestinal epithelial cells. *Sci Rep* 2016; 6:36795.
4. Miyoshi H, Stappenbeck TS. In vitro expansion and genetic modification of gastrointestinal stem cells in spheroid culture. *Nat Protoc* 2013;8:2471-2482.
5. Lipinski S, Grabe N, Jacobs G, et al. RNAi screening identifies mediators of NOD2 signaling: implications for spatial specificity of MDP recognition. *Proc Natl Acad Sci U S A* 2012;109:21426-21431.
6. Livak KJ, Schmittgen TD. Analysis of relative gene expression data using real-time quantitative PCR and the 2(-Delta Delta C(T)) method. *Methods* 2001; 25:402-408.
7. Adolph TE, Tomczak MF, Niederreiter L, et al. Paneth cells as a site of origin for intestinal inflammation. *Nature* 2013;503:272-276.
8. Niederreiter L, Fritz TM, Adolph TE, et al. ER stress transcription factor Xbp1 suppresses intestinal tumorigenesis and directs intestinal stem cells. *J Exp Med* 2013;210:2041-2056.
9. Howell KJ, Kraiczy J, Nayak KM, et al. DNA methylation and transcription patterns in intestinal epithelial cells from pediatric patients with inflammatory bowel diseases differentiate disease subtypes and associate with outcome. *Gastroenterology* 2018;154:585-598.

B

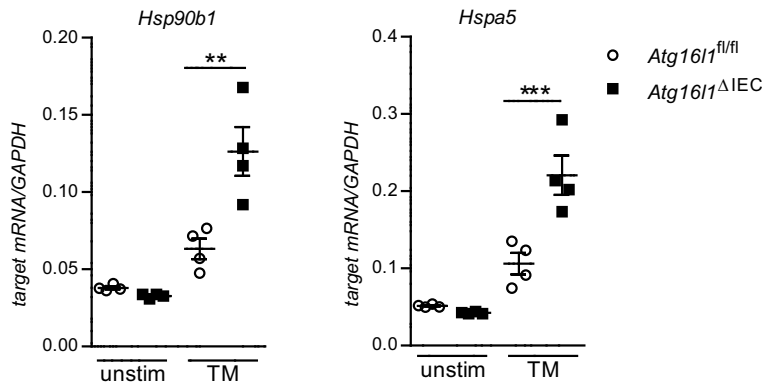


Supplementary Figure 1. Systematic siRNA screening identifies modulators of the ATF6 branch. (A) Network of candidate genes after the primary screen based on STRING. Only interactions with a confidence score >0.4 were considered. $P = .00147$. (B) Schematic cellular localization of the 6 ATF6 α modulators subjected to further functional studies. ATF6 signaling inducers are depicted in *green*, inhibitors shown in *orange*.

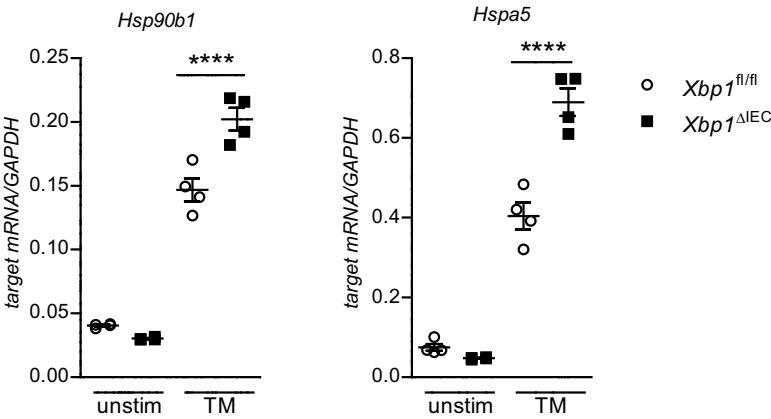


Supplementary Figure 2. Hyperactivation of the non-canonical NF- κ B signaling in *Atf6* transgenic intestinal organoids. (A) Knockdown efficiency for *ATF6*, *ACSL1*, and *CSNK2B* in Caco-2 cells was calculated (related to B). Samples treated with the nontargeting siRNA (scrambled, unstimulated) were set to 1. (B) Transcript levels of NF- κ B signaling components in SI organoids treated with tunicamycin (TM 100 ng/mL) for 24 hours. (C) Immunoblotting of protein lysates collected from WT and *Atf6* tggt SI organoids stimulated with Tunicamycin (TM, 100 ng/mL). Relative p-p65, p52, and p-p38 protein levels were quantified. The average value of the unstimulated WT controls was set to 1. N = 3 biological replicates. (D) *cIAP1/Birc2* and *cIAP2/Birc3* mRNA levels in WT and *Atf6* tggt SI organoids stimulated for 24 hours. Related to [Figure 3B](#). Depicted data representative of 3 independent experiments. For statistical analysis, 1-way analysis of variance together with Tukey post hoc test was performed.

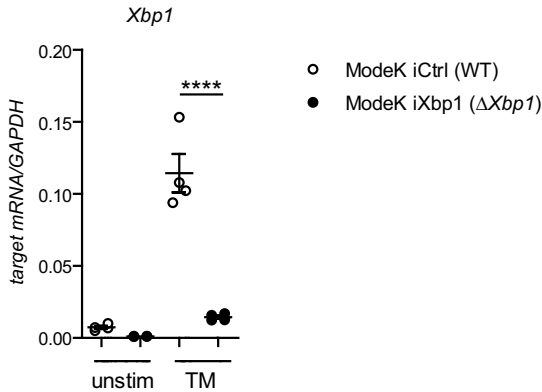
A



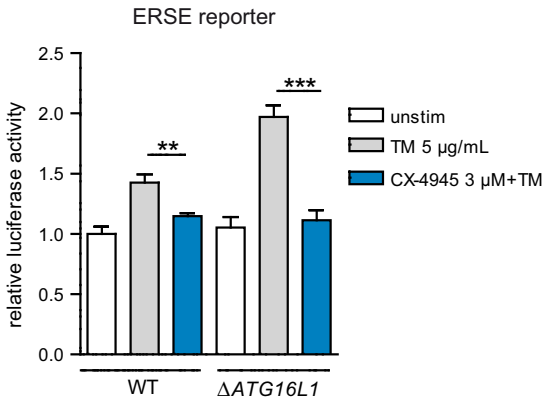
B



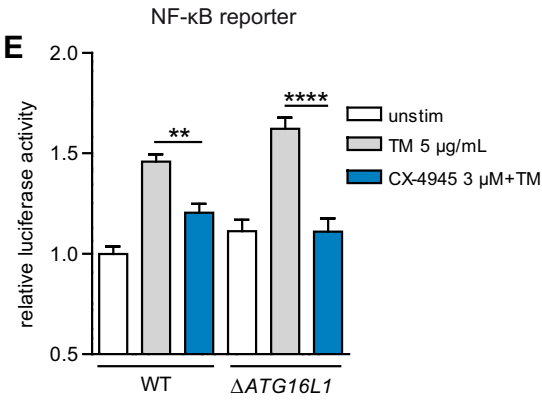
C



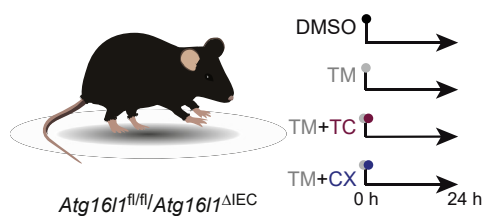
D



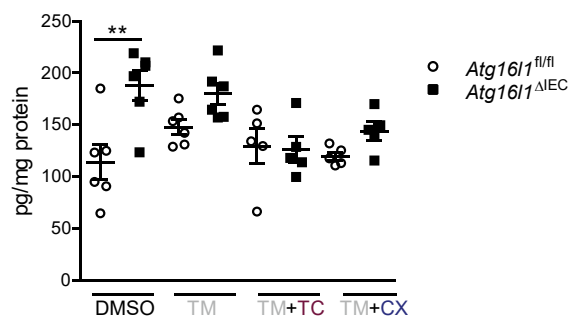
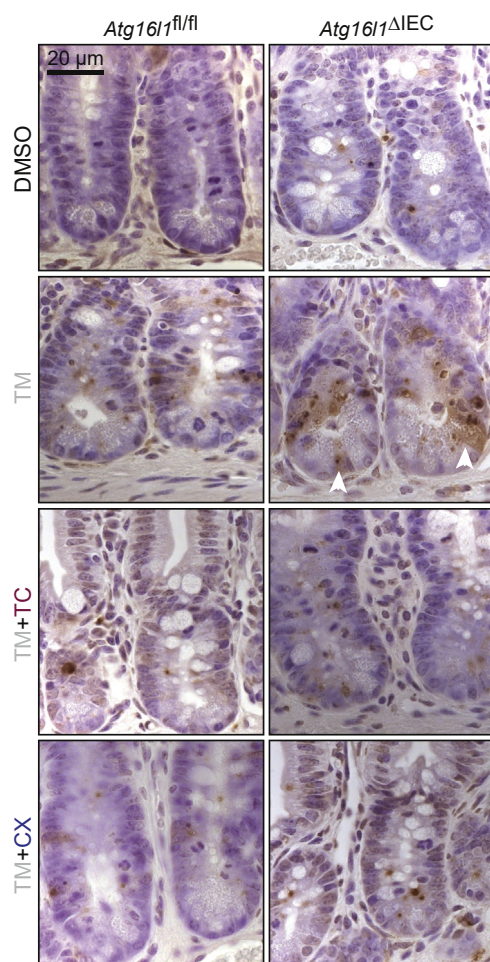
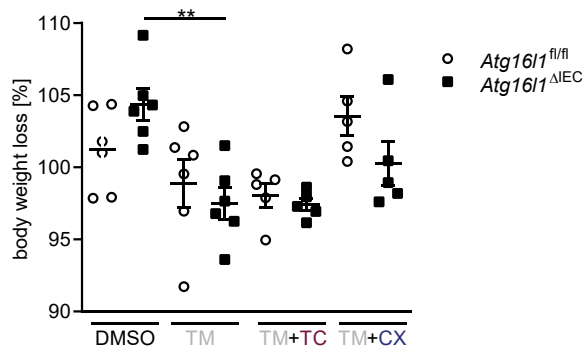
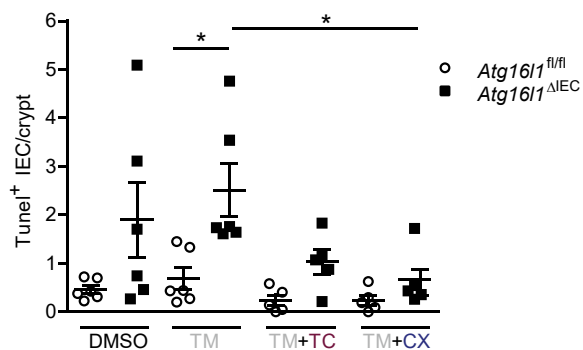
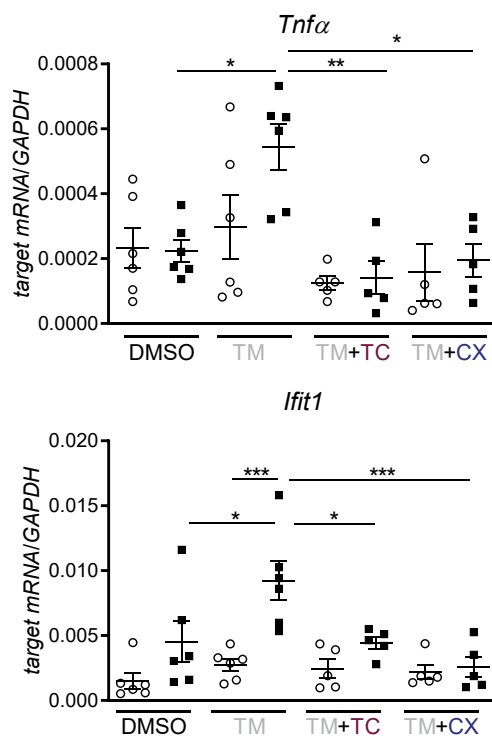
E

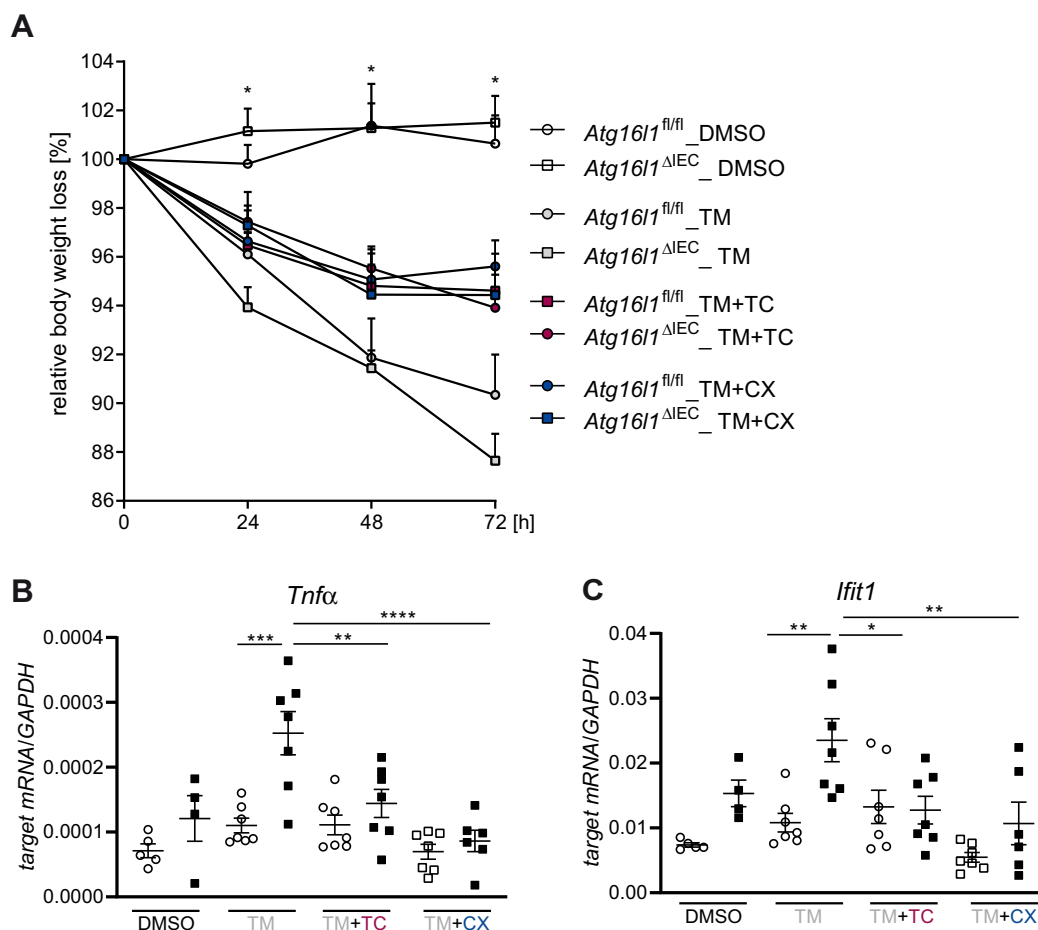


Supplementary Figure 3. Hyperactivation of the ATF6 α branch in *Atg16l1*- and *Xbp1*-deficient small intestinal organoids. Transcript levels of *Atf6 α* target genes *Hsp90b1* (*Grp94*) and *Hspa5* (*Grp78*) in small intestinal organoids treated with tunicamycin (TM, 100 ng/mL) for 24 hours. (A) *Atg16l1*^{fl/fl} and *Atg16l1* ^{Δ IEC} SI organoids. n = 4 biological replicates. (B) *Xbp1*^{fl/fl} and *Xbp1* ^{Δ IEC} small intestinal organoids. n = 4 biological replicates. (C) Transcript levels of *Xbp1* in *Xbp1*-deficient MODE-K cells (n = 4). (D) ERSE promoter activity and (E) NF- κ B luciferase activity in Caco-2 cells on exposure to tunicamycin (5 μ g/mL) for 24 hours in the presence or absence of CX-4945 (3 μ M) as indicated. Shown data representative of 3 independent experiments. For statistical analysis, 1-way analysis of variance together with Tukey post hoc test was performed.

A**C**

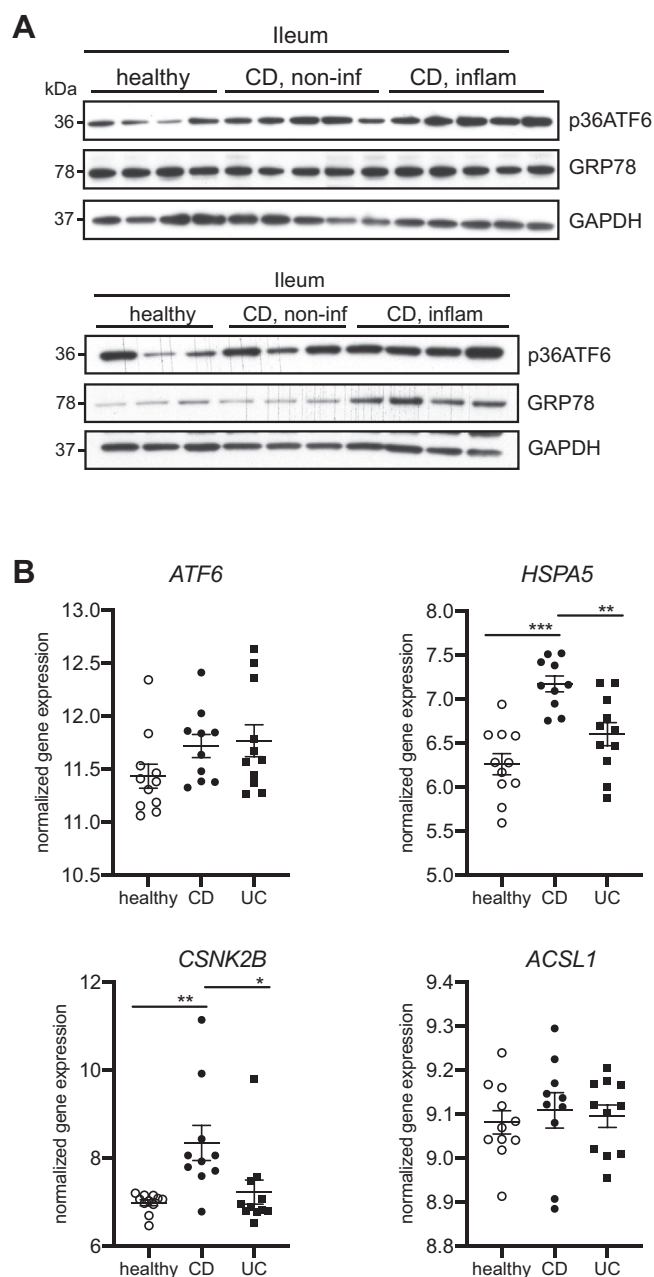
CXCL1 ELISA SI Crypts

**D****B****E****F**



Supplementary Figure 5. Inhibition of the ATF6 α branch reduces ER-stress mediated proinflammatory signaling in $Atg16l1^{\Delta IEC}$ mice after 72 hours of treatment. Mice received 1 mg/kg bodyweight of tunicamycin IP, when indicated mice were additionally treated with either TC (2.5 μ g/g bodyweight) or CX-4945 (40 μ g/g bodyweight) at 0, 24, and 48 hours. Control groups received dimethyl sulfoxide (DMSO). Mice were killed after 72 hours ($n = 4/7$). (A) Body weight loss. (B) Transcript levels of *Tnfα* and *Ifit1* in SI crypt lysates of $Atg16l1^{fl/fl}$ and $Atg16l1^{\Delta IEC}$ mice after 72 hours of treatment. Statistical analysis was performed using 1-way analysis of variance together with Tukey post hoc test.

Supplementary Figure 4. Restriction of the ATF6 α branch reduces ER-stress mediated inflammation and cell death in $Atg16l1^{\Delta IEC}$ mice. (A) Stimulation scheme of $Atg16l1^{fl/fl}$ and $Atg16l1^{\Delta IEC}$ mice ($n = 5/6$). Mice were treated with 1 mg/kg bodyweight of tunicamycin IP, when indicated mice additionally received either TC (2.5 μ g/g bodyweight) or CX-4945 (40 μ g/g bodyweight). Control groups received dimethyl sulfoxide (DMSO). After 24 hours, mice were killed. (B) Weight loss 24 hours after injection. (C) CXCL1 concentration in SI crypt lysates detected via enzyme-linked immunosorbent assay. (D and E) TUNEL staining of SI sections with representative pictures (D) and quantification (E). A minimum of 50 crypts/intestine were assessed in each treatment group. Bars = 20 μ m. Arrowheads show apoptotic Paneth cells. (F) Transcript levels of *Tnfα* and *Ifit1* in SI crypt lysates of treated $Atg16l1^{fl/fl}$ and $Atg16l1^{\Delta IEC}$ mice after 24 hours. Statistical analysis was performed using 1-way analysis of variance together with Tukey post hoc test.



Supplementary Figure 6. Enhanced ATF6 signaling in patients with IBD. (A) Immunoblotting of protein levels of p36ATF6 and GRP78 derived from SI organoid lysates generated from healthy (n = 7), CD noninflamed (n = 8), and CD inflamed tissue (n = 9). Related to [Figure 7B](#). (B) Relative mRNA expression of *ATF6*, *HSPA5*, *ACSL1*, and *CSNK2B* in IECs from ileal biopsies from pediatric patients with IBD (CD, n = 10 and UC, n = 11) and healthy controls (n = 11) (data obtained from Howell et al.⁹). Differential expression calculated between control and diseased using DE-Seq2. Statistical analysis was performed using 1-way analysis of variance together with Tukey post hoc test.